Climate Dynamics
https://doi.org/10.1007/s00382-024-07359-z

ORIGINAL ARTICLE

The atmospheric effect of aerosols on future tropical cyclone frequency and precipitation in the Energy Exascale Earth System Model

Ana C. T. Sena[1] · Christina M. Patricola[1,2] · Suzana J. Camargo[3] · Adam H. Sobel[3,4]

Received: 22 March 2024 / Accepted: 19 July 2024

Abstract
This study uses experiments from the Energy Exascale Earth System Model (E3SM) to compare the influence on tropical cyclone (TC) activity of: (i) the atmospheric effect of aerosols under specified sea-surface temperatures (SSTs); and (ii) the net effect of greenhouse gases (GhGs) (including changes in SSTs). The experiments were performed using the CMIP6 Shared Socioeconomic Pathway SSP5-8.5 emissions scenario with GhG-induced SST warming specified and atmospheric aerosol effects simulated but without explicit ocean coupling. Insignificant changes in global TC frequency are found in response to the atmospheric effect of future aerosols and GhGs, as significant regional responses in TC frequency counteract each other. Future GhGs contribute to more frequent TCs in the North Atlantic, and reductions over the Northwestern Pacific and Southern Indian Ocean. The atmospheric effect of future aerosols drives more frequent TCs over the Northwestern Pacific and reductions over the Northeast Pacific and North Atlantic. Along with increases in TC intensity, global TC precipitation (TCP) is projected to increase by 52.8% (14.1%/K) due to the combined effect of future aerosols and GhGs. Although both forcings contribute to TCP increases (14.7–19.3% from reduced aerosols alone and 28.1–33.3% from increased GhGs alone), they lead to different responses in the spatial structure of TCP. TCP increases preferentially in the inner-core due to increased GhGs, whereas TCP decreases in the inner-core and increases in the outer-bands in response to the atmospheric effects of decreased aerosols. These changes are distinct from those caused by aerosol-induced SST changes, which have been considered in other studies.

Keywords Tropical cyclones · Climate change · Anthropogenic aerosols · Tropical meteorology · Extreme events

1 Introduction

Tropical cyclones (TCs) are among the most destructive natural disasters, with several events, including Hurricanes Katrina (2005), Harvey (2017), and Ian (2022), each causing economic damages exceeding $100 billion dollars (NOAA 2022). There is growing evidence that TCs are affected by anthropogenic climate change. The fraction of TCs reaching high intensities in the observational record has been increasing (Knutson et al. 2019; Kossin et al. 2020; Klotzbach et al. 2022; Camargo et al. 2023), and this trend is projected to continue with future warming

Suzana J. Camargo and Adam H. Sobel have contributed equally to this work.

✉ Ana C. T. Sena
anasena@iastate.edu

Christina M. Patricola
cmp28@iastate.edu

Suzana J. Camargo
suzana.camargo@columbia.edu

Adam H. Sobel
ahs129@columbia.edu

[1] Department of the Earth, Atmosphere, and Climate, Iowa State University, 716 Farm House Ln, Ames, IA 50011, USA

[2] Climate and Ecosystem Sciences Division, Lawrence Berkeley National Laboratory, 1 Cyclotron Rd, Berkeley, CA 94720, USA

[3] Lamont-Doherty Earth Observatory, Columbia University, 61 Rt. 9W, Palisades, NY 10964, USA

[4] Department of Applied Physics and Applied Mathematics, Columbia University, 500 W 120th St., New York, NY 10027, USA

Published online: 13 August 2024

(Walsh et al. 2016; Knutson et al. 2020; Camargo et al. 2023). There is lower confidence in the projected changes in TC frequency. While some studies suggest that the total number of global TCs has been decreasing in the observational record (Knutson et al. 2019; Klotzbach et al. 2022; Chand et al. 2022), there is no consensus on how global TC frequency may change in the future, as studies suggest no significant change or small decreases in the global number of TCs by the end of the 21st century (Vecchi et al. 2019; Knutson et al. 2020; Sobel et al. 2021). Similarly, there is no consensus on regional basin-wide trends. While there are some trends found in observations, such as more frequent TCs in the North Atlantic and less frequent TCs in the Northwestern Pacific and Northeast Pacific, the attribution of these trends to climate change is not clear, partially due to the effect of multidecadal variability and improvements in observations (Walsh et al. 2016; Murakami et al. 2020; Klotzbach et al. 2022; Chan and Liu 2022), as well as uncertainties in the pattern of forced SST change (Sobel et al. 2023).

Global trends in TC frequency are influenced primarily by two external forcings: greenhouse gases (GhGs) and aerosols (e.g., Mann and Emanuel 2006; Booth et al. 2012; Dunstone et al. 2013; Ting et al. 2015; Sobel et al. 2016, 2019). While GhGs concentrations have been steadily increasing during the observational record, aerosol emissions have followed a different trajectory. Anthropogenic aerosol emissions increased during most of the 20th century but have been decreasing since the 1980s, with the greatest reductions observed in Europe and North America. During the historical period, increasing aerosol concentrations counteracted the effect of GhG emissions on TC genesis, as GhG-induced warming increases the potential intensity of TCs, while aerosol-induced SST cooling contributes to a reduction in potential intensity (Sobel et al. 2016). Aerosol cooling is approximately twice as effective as GhG-induced warming in changing the potential intensity of TCs per degree Celsius of sea surface temperature (SST) warming, due to differences between shortwave and longwave forcings on potential intensity (Mann and Emanuel 2006; Booth et al. 2012; Dunstone et al. 2013; Emanuel and Sobel 2013; Sobel et al. 2019; Rousseau-Rizzi and Emanuel 2022); it can be three times more effective than GhGs in causing PI changes over the North Atlantic (Ting et al. 2015). As aerosol emissions are not evenly distributed around the globe, there is evidence that the increase in aerosols emissions during the 20th century led to a less favorable environment for TC genesis in the Northern Hemisphere, where most of the anthropogenic aerosol emissions are located, due to changes in the atmospheric circulation such as greater vertical wind shear and descending motion when compared to the pre-industrial period, while the opposite is true for the Southern Hemisphere (Cao et al. 2021).

Since the 1980s aerosol emissions have been decreasing, especially over Europe and North America. This reduction caused regional changes in the global distribution of TCs (Dunstone et al. 2013; Takahashi et al. 2017; Murakami 2022b), relative warming of the Main Development Region (MDR), and a northward shift of the Inter-Tropical Convergence Zone (ITCZ). As a result, TC seasons were more active in the 1980s than they would have been without the decline in aerosol emissions (Dunstone et al. 2013). Note that long-term trends of Atlantic TCs are difficult to assess due to the competing effect of modes of climate variability, such as the Atlantic Multidecadal Variability (AMV, Goldenberg et al. 2001; Emanuel 2005). While there is an ongoing debate on whether aerosols are a primary force on driving the AMV (e.g. Zhang et al. 2013; Murphy et al. 2017, 2021), the Atlantic Overturning Circulation has also been suggested as a driver of the decline of the number of major hurricanes over the North Atlantic in 2005–2015, when only modest changes in aerosol emissions occurred (Yan et al. 2017). In the Northwestern Pacific, local changes in aerosol concentrations led to a reduction in TC frequency due to increased vertical wind shear and decreased vorticity in the region (Takahashi et al. 2017). According to Murakami (2022b), the observed reductions of aerosol concentrations over the western hemisphere led to an increase in TC frequency in the North Atlantic and decreases in the Southern Hemisphere and NWP. They suggested two pathways for these changes: (1) a thermodynamic pathway, by which increased aerosol loading over the ocean reduces solar insolation leading to cooler oceans, weakening TC activity; and (2) a dynamic pathway, by which the reduction of aerosol loading leads to anomalous mid-latitude heating in the Northern Hemisphere and to a poleward shift of the subtropical jets, altering vertical wind shear. Meanwhile, the anomalous ascending motion over the Northern Hemisphere leads to subsidence anomalies over the Southern Hemisphere, decreasing TC frequency in the region. In the present study, we analyze how future changes in aerosol distribution may affect TC frequency under fixed SST, thus in the absence of the thermodynamic effect.

In addition to TC frequency, it is important to include precipitation in considering the potential for TCs impacts in a future warming climate. Even though TCs are categorized by their maximum sustained wind speeds (Saffir–Simpson scale), water-related hazards are responsible for about 88% of TC-related fatalities in the United States, with flooding being the second greatest cause of deaths in the 1963–2012 period (Rappaport 2014). The importance of TC precipitation has been recognized and there are proposed methods on how to include rainfall and storm surge measurements of severity (e.g. Bloemendaal et al. 2021). As such, reliable projections of future changes in TC precipitation (TCP) can provide valuable information to mitigate these hazards.

An increase in TCP is already apparent in observations (e.g. Guzman and Jiang 2021; Tu et al. 2021; Traxl et al. 2021; Shearer et al. 2022), though this wetting is limited to the outer-bands of the TC, while there is a reduction in the observed precipitation in the inner-core of the TC, in the 1998–2019 satellite observations (Guzman and Jiang 2021; Tu et al. 2021). TCP is projected to become more intense in a warmer climate (e.g. Scoccimarro et al. 2014; Patricola and Wehner 2018, and references therein). These changes are partially due to a greater moisture holding capacity in the atmosphere with warming. The Clausius–Clapeyron relation indicates that for any given 1 °C warming, the moisture saturation in the atmosphere should increase by about 7%. Indeed, the median projected increase in hurricane precipitation with a 2 °C warming is about 14%, consistent with Clausius–Clapeyron (Knutson et al. 2020). However, the increased rainfall rates in some models far exceed this simple theoretical estimate, with some studies suggesting TC rainfall may increase by double the theoretical change (Knutson et al. 2013; Villarini et al. 2014; Knutson et al. 2015; Liu et al. 2019). TC intensification has been suggested as responsible for part of this wetting (Liu et al. 2019; Stansfield and Reed 2021), with an estimated 12% of the accumulated TCP increase associated with more intense TCs (Stansfield and Reed 2021). This intensity-related enhancement is similar to what has been proposed for other sorts of precipitation extremes, because increased precipitation (e.g., due to the water vapor increase) leads to stronger vertical motion, which increases precipitation further (e.g. Nie and Sobel 2016; Nie et al. 2018).

Aerosols have been suggested to change the structure of TCs, which can impact TC precipitation and intensity. Studies using convection permitting models suggest that an excess of aerosols increases the number of cloud condensation nuclei in the peripheral clouds, delaying precipitation as the collision and coalescence process is initially suppressed (Krall and Cottom 2012; Wang et al. 2014). Later, it invigorates convection in the outer bands of the TC, while weakening the convergence in the center of the storm and thus, the intensity of the TC (Rosenfeld et al. 2012; Krall and Cottom 2012). This results in weaker TCs, but with stronger precipitation due to a larger rainband, partially due to enhanced latent heat in this region (Wang et al. 2014; Zhao et al. 2018). Conversely, TCs formed in a clean aerosol regime are usually more intense than the ones formed in polluted states in convection-permitting simulations (Hazra et al. 2013).

As clean air policies are developed and reinforced, a further decrease in aerosol emissions is expected in the future, especially over Asia. The Coupled Model Intercomparison Project Phase 6 (CMIP6, Eyring et al. 2016) includes five main narratives for the future of climate change scenarios, known as Shared Socioeconomic Pathways (SSP; Riahi et al. 2017). Each narrative is associated with a different Representative Concentration Pathway (RCP), that describes the expected radiative forcings, both from GhGs and aerosols. These scenarios range from a high mitigation scenario, with the projected change meeting the goal of limiting the global warming to around 1.5 °C by 2100 (SSP1-1.6; van Vuuren et al. 2017), to a worst case scenario, with high emissions and no mitigation scenario, where global warming can reach over 5 °C by 2100 (SSP5-8.5; Kriegler et al. 2017) (IPCC 2021). In all CMIP6 future scenarios, with the exception of SSP3 (Fujimori et al. 2017) and SSP4 (Calvin et al. 2017), aerosols are projected to decrease in the future (Rao et al. 2017; Fiedler et al. 2019; Lund et al. 2019). In most studies that assess projected changes in TC activity, the increase in GhG radiative forcing and the reduction in aerosol emissions occur simultaneously (e.g. Roberts et al. 2020; Knutson et al. 2020). In this study, we aim to decouple the regional effects of the projected changes in TC activity derived from aerosols from the GhGs effect in the CMIP6 SSP5-8.5 scenario, using atmospheric-only idealized experiments from a TC-permitting resolution global climate model (E3SM). The SSP5-8.5 scenario is a high emission scenario, including a projected increase in radiative forcing of 8.5 W/m^2 by 2100, with a strong fossil-fuel based development and increases in GhGs concentrations, while the enforcement of policies against pollution and the development of new technologies leads to reductions in aerosol emissions (Kriegler et al. 2017). Note that the SSP5-8.5 can be considered unrealistic as it requires large increases in GhGs emissions and coal consumption that do not seem plausible given the current trends in GhGs emissions (Hausfather and Peters 2020). However, the most likely middle-of-the-road scenarios for radiative forcings, SSP3 (Hausfather and Peters 2020), has higher aerosol emission rates than the high emissions scenarios (SSP5) (Rao et al. 2017; Lund et al. 2019). As our objective is to explore the contribution of atmospheric effects of the aerosols, we chose a scenario with both high GhGs concentration and low aerosol emissions.

The ability of aerosols to modulate TC activity is commonly explained by the fact that a greater aerosol burden leads to a greater scattering of direct radiation, leading to SST cooling and a less favorable environment for TC genesis and intensification. While recognizing the importance of this mechanism, here we focus on the impact of aerosols on TC activity under constant SSTs. A similar method has been used to estimate the direct effect of carbon dioxide (CO_2) on climate change projections, and highlighted the importance of the atmospheric effects of the increase in GhGs. Bony et al. (2013) has suggested that approximately half of the projected changes in tropical precipitation are independent of the surface warming. Instead, these changes can be attributed to the direct effects of the increases in CO_2 concentration, associated with weaker radiative cooling leading to

anomalous atmospheric circulation. While Chadwick et al. (2014) suggested that the change in patterns of SST has a greater influence on the regional distribution of the precipitation response to abrupt $4 \times CO_2$ climate scenarios, they suggest that the direct effect of the CO_2 may have contributed to the mean changes in the tropical circulation and rainfall changes, partially due to changes in the land-sea temperature gradient. The direct atmospheric effects of CO_2 have also been suggested to affect TC frequency. Yoshimura and Sugi (2005) suggested that a uniform 2K warming alone in global SST can reduce TC frequency by about 6%, whereas this rate increases to 22% when the atmospheric effects of a doubling CO_2 concentration are considered. Using a similar experiment Held and Zhao (2011) found a 20% decrease in TC frequency in experiments with doubling CO_2 concurrent with a 2K uniform SST warming. They found that half of this response can be attributed to the increase in CO_2 under fixed SST, while simulations with a 2K SST warming can reproduce the other half. They also found that the relative importance of the CO_2 concentration and SST warming is regionally dependent, and attribute that to changes in atmospheric circulation, notably in mean vertical motion and mid-troposphere moisture due to the atmospheric effect of CO_2. TC intensification could only be reproduced with a SST warming in their experiments (Held and Zhao 2011).

Due to the relatively low residence time of anthropogenic aerosols, rapid variations in aerosol concentrations are more realistic than rapid changes in GhGs and it is reasonable to study the atmospheric effect of a reduction in aerosol emissions. Here, we explore how perturbations in the large-scale circulation caused by the future changes in GhGs and in aerosol emissions under the SSP5-8.5 scenario, excluding the effect of aerosols on SST, may affect projected changes in the frequency and regional distribution of TCs, the structure of TC precipitation, and TC environmental favorability.

2 Data and methods

2.1 Model description

A set of idealized atmosphere-only experiments were performed using the high resolution ($\approx$ 0.38°) energy Exascale earth system model (E3SM), version 2 (Caldwell et al. 2019a), with greenhouse gas (GhG) concentrations and aerosols emissions following the CMIP6 protocol (Eyring et al. 2016).

E3SM version 2 uses two main parameterization schemes to represent subgrid turbulent transport and cloud macrophysics (Golaz et al. 2022). The Cloud Layers Unified by Binormals parametrization (CLUBB, Golaz et al. 2002) is used for shallow cumulus clouds, with liquid cloud fraction and cloud liquid water diagnosed via a probability density function derived from subgrid moments of turbulence, heat content, and moisture. Meanwhile, the deep convection scheme is based on the scheme proposed by Zhang and McFarlane (1995), with updated dynamic constraints proposed by Xie et al. (2019). The parcel buoyancy is derived from the subgrid temperature obtained by the CLUBB scheme (Golaz et al. 2022). Aerosol representation in E3SM version 2 is based on the four-mode version of the Modal Aerosol Module (MAM4, Liu et al. 2016), with improvements on the characterization of aerosol-cloud and aerosol-radiation interactions (Golaz et al. 2019, 2022). The aerosol representation is characterized by four main modes: (1) Aitken, (2) accumulation, (3) coarse, and (4) primary carbon mode. While there is a general improvement in cloud characterization in E3SM version 2, Golaz et al. (2022) reported a bias in the cloud-aerosol interactions over mid and high latitudes, with unrealistically small cloud droplet number concentration frequently appearing under relatively clean aerosol conditions.

2.2 Experimental design

Four E3SM experiments will be considered in our analysis. A control historical simulation (CTLhist) was forced with fixed GhGs concentrations and aerosol emissions, such as black carbon, sufur dioxide, sulfates, primary organic matter and precursor gases, from the year 2010 following the historical CMIP6 protocol. SST and sea ice were imposed based on the monthly mean averages from the 1980–2010 period of the E3SM-DECK historical simulation (Golaz et al. 2019). Biases in the background climatological SST can lead to significant errors in TC activity in climate models (e.g., Hsu et al. 2019; Vecchi et al. 2019). Therefore in these simulations, the forcing field was bias-corrected by removing the monthly mean SST bias, defined as the difference between the monthly mean E3SM climatological SSTs and the monthly mean 1980–2010 climatology of the Hadley Centre Sea Ice and Sea Surface Temperature data set (HadISST, Rayner et al. 2003). The initial conditions for the atmospheric and land variables were derived from the end of the historical period of the E3SM-DECK experiments (associated with the year 2015), as described in Sena et al. (2022)

A control future simulation (CTLfut) was performed by imposing fixed GhG concentrations and aerosol emissions from 2100 based on the SSP5-8.5 emissions scenario. Monthly SST and sea ice were imposed based on the monthly mean climatology for 2070–2100 from the 1pctCO2 experiment of the E3SM-DECK simulation (Golaz et al. 2022). The 1pctCO2 experiment (Eyring et al. 2016) is based on gradual increase of 1% per year in the CO_2 emissions until quadrupling the emissions from 1850. As with the historical simulations, the monthly SST bias relative to the 1980–2010 HadISST climatology was removed. The initial conditions

for the atmospheric and land variables were derived from the end of the 21st century for the 1pctCO2 experiments in the E3SM-DECK, corresponding to the year 2100. Land use is the same in both experiments, set to year 2015 according to the CMIP6 protocol. Further details on the initialization of these experiments and on their performance compared to observations can be found in Sena et al. (2022).

Two additional new experiments were performed specifically for this study: (i) An experiment similar to CTLhist experiment except the aerosol emissions were set to the 2100 levels as in CTLfut (ghgHaerF); (ii) an experiment similar to CTLfut, but with 2010 aerosol emissions (ghgFaerH). The GhGs, aerosols, and SST forcing used in all experiments are summarized in Table 1. Thus, the difference between ghgFaerH and CTLhist and between CTLfut and ghgHaerF correspond to the response of TCs to future GhGs and SSTs, given historical and future aerosol levels, respectively. Similarly, the response to future aerosols emissions and their spatial distribution is identified by the difference between the ghgHaerF and CTLhist (for historical GhGs and SSTs) and CTLfut and ghgFaerH (for future GhGs and SSTs).

We use SO_2 emission rates and concentration as a proxy for changes in aerosols emissions, as SO_2 is suggested to have the greatest mean effective radiative forcing among the aerosol species changed in the 1850–2014 period (Thornhill et al. 2021). The annual mean change in SO_2 emission rate imposed in the future vs. historical climate is shown in Fig. 1. As mentioned above, a global reduction in aerosol emissions, with the greatest changes occurring over Asia, is assumed in the CMIP6 SSP5-8.5 future scenario. Note that changes in the SST forcing are based only on changes in GhGs, not aerosols. This is a simplification, as it is estimated that about 20% of the global temperature warming in the CMIP5 RCP8.5 scenario can be attributed to reductions in aerosol emissions (Westervelt et al. 2015; Xu et al. 2018). The RCP8.5 scenario is the high emissions scenario in the CMIP5 experiments (Taylor et al. 2012) corresponding to SSP5-8.5 in CMIP6, where the radiative forcing increases gradually since 2005, reaching 8.5 W/m^2 by the end of the 21st century. In these atmosphere-only experiments, SST responses to the changes in aerosol concentration are not accounted for, whereas the effects of aerosols on the atmosphere are simulated. Specifically, the experiments account for the direct effect of aerosols in the atmosphere and for changes in the large-scale circulation due to the atmospheric effects of the changes in global aerosol distribution, as well as for cloud-aerosol interactions simulated in E3SM version 2. Note that the future SST is derived from the 1pctCO2

Table 1 Summary of the E3SM experiments

	Aerosol emissions	GhGs concentration	SST
CTLhist	Historical (2010)	Historical (2010)	Historical (1980–2010)
ghgHaerF	Future (2100)	Historical (2010)	Historical (1980–2010)
ghgFaerH	Historical (2010)	Future (2100)	Future (2070–2100)
CTLfut	Future (2100)	Future (2100)	Future (2070–2100)

GhG concentrations and aerosol emissions were prescribed from the year 2010 for the historical period, and the year 2100 according to the SSP5-8.5 pathway in CMIP6 for the future. Monthly sea surface temperature (SST) was imposed based on the bias-corrected monthly mean SST for the 1980–2010 period in the historical simulations and the 2070–2100 period for the 1pctCO2 in the E3SM-DECK

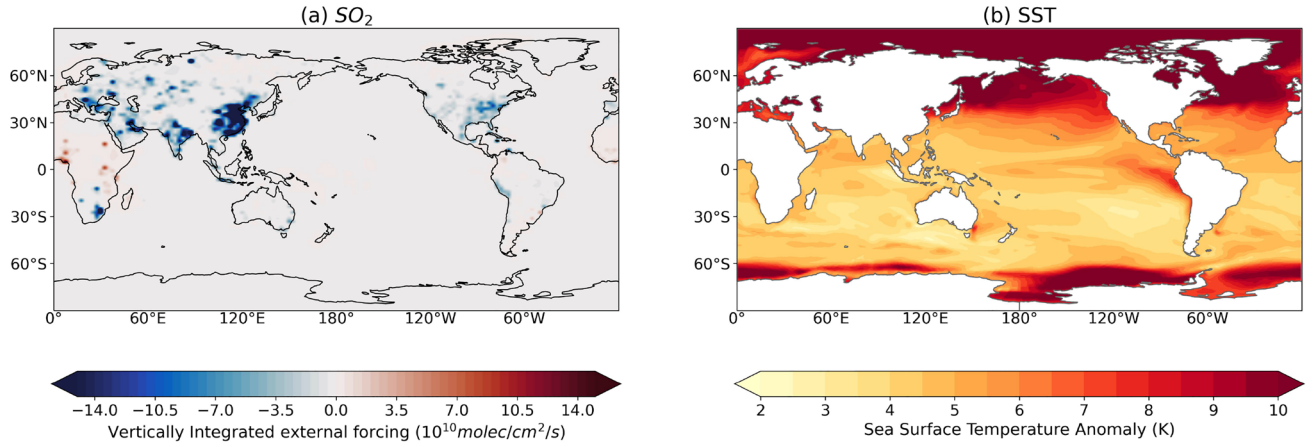

Fig. 1 Difference between the future minus historical August–September–October (ASO) averaged **a** vertically integrated external forcing for SO_2 (10^9 molecules/cm^2/s) and **b** sea surface temperature (K) imposed in the future experiments

scenario while the experiments in this study are based on the SSP5-8.5 scenario. As a result, the SST change in this protocol may be stronger than what would be expected from the SSP5-8.5 scenario alone as the CO_2 concentration reaches 1265 ppm for 1pctCO2, while the it is 1140 ppm for the SSP5-8.5 scenario by 2100.

Each experiment was initialized on April 1 and run for one year, with model output saved at a 6-hourly temporal frequency. Ten realizations of each experiment were performed, differing only by a round-off error in the initial temperature field, totaling an ensemble of ten runs for each experiment.

The global distribution of TCs in the E3SM model is reasonably reproduced in the historical control simulations when compared with observations, while TC intensity is underestimated, partially due to the spatial resolution considered (Davis 2018; Balaguru et al. 2020; Sena et al. 2022).

2.3 TC identification and definition of environmental variables

Simulated TCs were identified using the Toolkit for Extreme Climate Analysis (TECA; Prabhat et al. 2012), based on the TC tracking algorithm by Vitart and Stockdale (2001). TCs are detected as disturbances with a maximum relative vorticity greater than $1.6 \times 10^{-4}\ s^{-1}$, a local minimum sea level pressure, and a warm core, with a local mean temperature between 300 and 500 hPa at least 0.8K greater than its adjacent areas (Prabhat et al. 2012). The first location where these conditions are met is considered the point of TC genesis. TCs are classified according to their region of formation, using the definitions of basins used by Prabhat et al. (2012). Only TCs with duration greater than 2 days are considered. As there is evidence that TCs have been migrating poleward with climate change (e.g. Kossin et al. 2014; Daloz and Camargo 2018), we chose to analyze all TCs found by the algorithm, not limiting to the ones formed in the tropics. An additional analysis was made using only TCs that formed over the tropics and subtropics, defined as $40°S$ to $40°N$.

To quantify TC characteristics, we calculated additional metrics including (1) accumulated cyclone energy (ACE; $10^4 kt^2$, or 10^4 squared knots), which is defined as the square of the maximum sustained wind every 6-hours, summed over the TC lifetime, and (2) TC intensity according to the Saffir–Simpson scale, which is based on the intensity of the maximum sustained wind. TCs that reached category 3 or greater are referred to as "major TCs."

In addition, we evaluated several indicators of large-scale environmental favorability for TCs including the Genesis Potential Index (GPI; Camargo et al. 2007; Emanuel and Nolan 2004), which is used to estimate how favorable the atmosphere and SST are to TC development. GPI is an empirical index, calculated by:

$$GPI = |10^5\eta|^{\frac{3}{2}} \left(\frac{RH}{50}\right)^3 \left(\frac{PI}{70}\right)^3 \left(1 + 0.1V_{shear}\right)^{-2} \quad (1)$$

where η is the absolute vorticity at 850 hPa (s^{-1}); RH is the mid-tropospheric relative humidity at 600 hPa (%), V_{shear} is magnitude of the vertical wind shear between the horizontal wind at 850 and 200 hPa (m/s); and PI is the potential intensity of the tropical cyclone (m/s), as defined by Emanuel (1988).

Note that while GPI is useful to summarize information from multiple variables, future changes in GPI may not directly correspond to changes in TC frequency in CMIP5 models (Camargo 2013). Typically GPI increases with anthropogenic climate change, while in most high-resolution models TC frequency decreases. This behavior is dependent on the variables used in the genesis index, as well as the genesis index formulation, see e.g. Camargo et al. (2014).

We also analyzed the dynamical genesis potential index (DGPI; Murakami and Wang 2022), an empirical index for TC genesis based solely on dynamic variables, calculated as:

$$DGPI = \left(2 + 0.1 \times V_{\text{shear}}\right)^{-1.7} \cdot \left(5.5 - \frac{du_{500}}{dy} \times 10^5\right)^{2.3} \cdot \left(5.0 - 20 \times \omega_{500}\right)^{3.4} \cdot \left(5.5 + \left|10^5\eta\right|\right)^{2.4} \cdot e^{-11.8} - 1.0 \quad (2)$$

where ω_{500} is the pressure vertical velocity of the wind at 500 hPa (Pa/s), u_{500} is the zonal wind at 500 hPa (m/s) and $-du_{500}/dy$ is the meridional shear vorticity associated with the zonal wind (1/s).

Responses in TC frequency and environmental variables are considered significant when they are different at or above the 95% confidence interval according to the two-tailed student-t test, unless noted otherwise.

2.4 Definition of tropical cyclone precipitation

We analyzed the following diagnostics of TC precipitation (TCP):

(i) The total precipitation in the TC (totalTCP), defined as the total precipitation within 500 km from the center of the TC (e.g. Prat and Nelson 2013; Khouakhi et al. 2017) through its lifetime.
(ii) The radially-averaged precipitation at 25 km, 50 km, 100 km, 400 km, and 500 km from the center of the TC (TCP25 km, TCP50 km, TCP100 km, TCP400 km, and TCP500 km, respectively). These radii were chosen to represent the the inner-core (25 km and 50 km), rainbands (100 km), and outer-bands (400 km and 500 km) of the TCs.
(iii) The azimuthally-averaged TCP was calculated from 25 km to 600 km from the center of the TC in 25 km

increments, to facilitate study of the spatial structure of TCP (e.g. Lonfat et al. 2004; Moon et al. 2022b).

Each TC is considered an independent event, and the mean value of each environmental variable following the TC in a 6-hourly timescale is calculated as the mean for all TCs in all 10-member ensembles for each experiment. The SST at the point of formation of each TC is used to calculate the rate of change of TCP per degree of SST change considering all TCs in each experiment. The uncertainty of these values is defined as the 95% confidence interval considering all TCs, in all 10-member ensembles for each experiment.

3 Results

3.1 Response in global tropical cyclone activity to GhGs and the atmospheric effect of aerosols in combination and individually

Our results indicate that neither the atmospheric effect of future aerosols nor GhGs have a significant effect on the global frequency of TCs. Furthermore, there is no significant change in global TC frequency when there is a concurrent change in aerosols and GhGs. The ensemble mean global TC frequency is 104.2 TCs/year in the ghgHaerF experiment, and 114.6 TCs/year in the CTLhist experiment, but the changes were statistically insignificant at the 95% confidence level (Fig. 2a and Table 2). When we considered only TCs generated over the tropics and subtropics, the number of TCs in the CTLhist is significantly greater than in the other experiments, by about 10 TCs/year or 11%. No other significant changes in the global TC number were found (Appendix Table 6).

Similarly, we did not find significant differences in the total TC number in the Northern Hemisphere in response to future aerosols, future GhGs, or both (Appendix Fig. 10a). In the Southern Hemisphere, there is a significant reduction in the total TC number in the ghgFaerH experiment compared to CTLhist, suggesting a possible reduction in TC frequency due to the effect of GhGs given historical aerosols (Appendix Fig. 10b). No other significant changes were found for the total TC frequency in the Southern Hemisphere.

In contrast, the number of major hurricanes, defined as category 3 or above, significantly increases in the future due to the combined GhG and aerosol forcings, with contributions from both GhG concentrations and the atmospheric

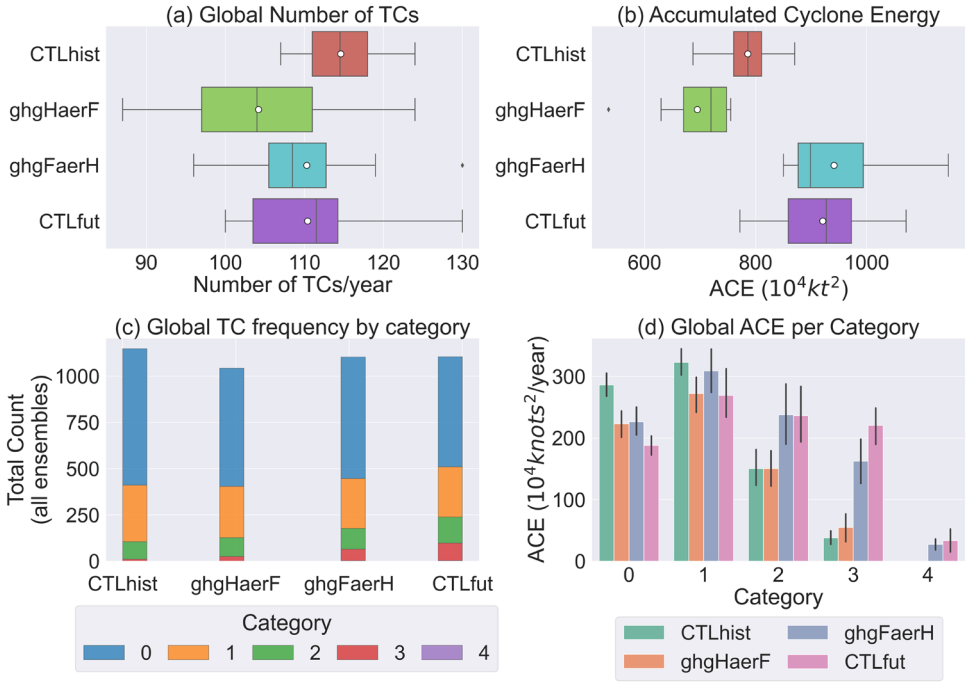

Fig. 2 **a** Total global number of tropical cyclones per year for each E3SM experiment; **b** Global mean accumulated cyclone energy per year (10^4 kt^2); The boxplot represents the internal atmospheric variability of the 10-member ensemble in each experiment. The edges of the boxplots show the 25th and 75th percentiles. Whiskers represent 1.5 the interquartile range. Outliers are marked with diamond-shaped symbols. The median is marked as a straight line, and the mean is noted by a white circle in panels **a**, **b**. **c** Total number of global TCs in the 10-member ensemble of each experiment. TCs are grouped by intensity based on the Saffir–Simpson scale, with category zero representing TCs that do not reach the threshold of hurricane strength. **d** Contribution of the intensity of the TC (based on the Saffir–Simpson scale) for the mean seasonal ACE (10^4 kt^2) in each experiment. The error bars represent one standard deviation from the mean based on all detected TCs

Table 2 Ensemble mean global number of TCs in each experiment, grouped by intensity according to the Saffir–Simpson category, and the percentage of major TCs, defined as the number of TCs classified as category 3 or above divided by the total number of TCs

Experiment	Total	cat0	cat1	cat2	cat3	cat4	Major (%)	ACE
CTLhist	114.6	73.5[all]	30.6	9.4[d]	1.1[all]	0.0	0.98[all]	785.7[all]
ghgHaerF	104.2	63.7[a]	27.8	10.2[d]	2.5[all]	0.0	2.47[all]	695.0[all]
ghgFaerH	110.3	65.6[a]	27.0	11.2[d]	6.3[all]	0.2	5.95[all]	941.1[a,b]
CTLfut	110.4	59.4[a]	27.2	14.0[all]	9.5[all]	0.3	8.88[all]	920.8[a,b]

The ensemble mean annual ACE (10^4 kt^2) is also shown. The values that are significantly different from each other at or above the 95% confidence level are represented by a superscript, with [a] representing values significantly different from CTLhist; [b] from ghgHaerF; [c] from ghgFaerH; and [d] from CTLfut. When the values are significantly different from all the others, it is marked with [all]. No significant changes were found for the global total frequency of TCs

effect of the decline in aerosol emissions (Fig. 2c and Table 2). The average number of major TCs is 1.1 TCs/year in the CTLhist experiment, increasing by 1.4 TCs/year due to decreases in aerosol concentration (ghgHaerF), and by 8.7 TCs/year due to future GhGs, assuming constant aerosols (ghgFaerH). Similarly, there is an increase of 3.3 major TCs/year due to future aerosols given constant future GhGs (CTLfut minus ghgFaerH) and 7.3 major TCs/year due to future GhGs given constant future aerosols (CTLfut minus ghgHaerF). All changes in the number of major hurricanes are statistically significant. This suggests that while increases in GhGs concentration make a greater contribution to TC intensity, the atmospheric effects of the reduction in aerosol emissions in the future are also an important contributor to TC intensity changes. These results are maintained when considering only TCs formed over the tropics (Table 6).

Global ACE significantly increases in the future with the concurrent change in aerosols and GhGs (Table 2 and Fig. 2b), from $785 \times 10^4 kt^2$ in the CTLhist to $920 \times 10^4 kt^2$ in the CTLfut experiment. ACE also increases due to GhGs alone, with the values increasing by $155 \times 10^4 kt^2$ (or $\approx 20\%$) and $226 \times 10^4 kt^2$ (or $\approx 32\%$), given historical and future aerosols, respectively. This is mainly due to the greater contribution of stronger TCs to ACE due to future GhGs (Fig. 2d). There is a smaller, but statistically significant reduction in ACE due to the atmospheric effect of future aerosols given historical GhGs, due to a more moderate contribution of major TCs to ACE. No significant changes in ACE were found due to the atmospheric effects of aerosols given future GhGs.

3.2 Response in regional tropical cyclone activity to future greenhouse gases

While the changes in global TC frequency are small and insignificant, there are statistically significant regional changes in individual TC basins due to both the future increase in GhG concentrations and the decrease in aerosol emissions. In this section we will discuss the responses of TC activity and environmental variables due to changes in GhGs, based on the difference between the CTLfut relative to the ghgHaerF and the difference between the ghgFaerH and CTLhist experiments.

Future GhGs contribute to fewer TCs in the Northwestern Pacific (Fig. 3a, see also Table 3), with a reduction of 5.9 TCs/year given historical aerosols (ghgFaerH minus CTLhist) and 2.2 TCs/year given future aerosols (CTLfut minus ghgHaerF; the latter is insignificant at the 95% confidence level, but significant at the 90% confidence level). TC frequency is also significantly reduced in the Southern Indian Ocean (Fig. 3e), by 7.9 and 3.2 TCs/year given historical and future aerosols. This is largely compensated by the TC frequency increases in the North Atlantic (Fig. 3c), by 9.7 and 8.1 TCs/year given historical and future aerosols, respectively. We also found a significant poleward displacement of the latitude of maximum intensities of TCs in both hemispheres due to future GhGs (Appendix Fig. 15), consistent with what is found in the literature (Kossin et al. 2014; Sharmila and Walsh 2018; Daloz and Camargo 2018; Studholme et al. 2022) and attributed to the expansion of the Hadley circulation, that is commonly associated with regional changes in SST (e.g. Zhou et al. 2020).

Various environmental factors contribute to the changes in TC activity due to increased GhGs. The potential intensity increases overall in each hemisphere's summer (here defined as August–October, ASO, for the Northern Hemisphere), partially following SST warming (Fig. 4a and Appendix Fig. 11a). This, in conjunction with a reduction of vertical wind shear (Fig. 4b) and enhanced relative humidity in the mid-levels (Fig. 4d) over the tropical North Atlantic Ocean, generate a more favorable environment for TCs in these regions. In the North Atlantic, this is aided by an increase in absolute vorticity in the tropics (Fig. 4c). Though there is more mid-level drying in the Gulf of Mexico, the changes in the environmental conditions result in increases in GPI in the North Atlantic (Fig. 4e), that leads to overall increases in TC genesis in the region (Fig. 4f). Note that we consider TC genesis as the first point where the disturbance that generates the TC is identified, even if it is over land. The responses in

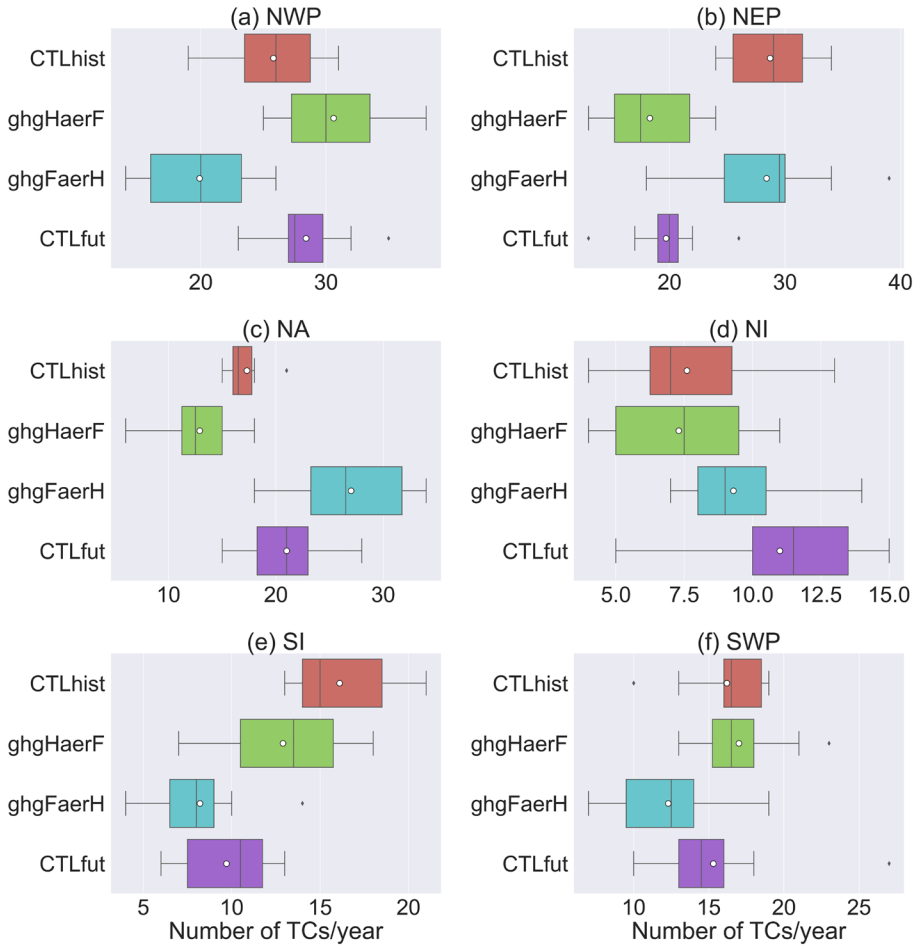

Fig. 3 Tropical cyclone frequency per year for each experiment for: **a** the Northwestern Pacific; **b** the Northeast Pacific; **c** the North Atlantic; **d** Northern Indian Ocean; **e** Southern Indian Ocean; **f** Southwestern Pacific. The boxplot represents the internal atmospheric variability of the 10-member ensemble in each experiment. The edges of the boxplots show the 25th and 75th percentiles. Whiskers represent 1.5 the interquartile range. The median is marked as a straight line, and the mean is noted by a white circle. Outliers are marked with diamond-shaped symbols

TC frequency are similar for all the basins if we restrict the analysis to TCs generated only over warm SSTs (not shown), as well as if we restrict our analysis to the tropics (Table 7). In the Northwest Pacific, there is mid-level drying in the tropics and negative anomalies in absolute vorticity off the eastern coast of Asia, contributing to an environment less favorable for TC development (Fig. 4c, d). Though some environmental variables in the Northwest Pacific act towards a more conducive environment for TCs, such as PI increases and reductions in vertical wind shear off the maritime continent, they do not seem to be enough to compensate the other effects (Fig. 4a, b). The environment becomes less favorable for TC development, as measured by both GPI (Fig. 4e) and DGPI (Fig. 12a), and TCs become less frequent in the region (Fig. 4f). Similar responses were found due to future GhGs given constant, historical aerosols (Appendix Fig. 11 and Fig. 12b).

In the Southern Hemisphere's summer (January to March, JFM), there is enhanced vertical wind shear and mid-level drying over the Southern Indian Ocean, leading to fewer TCs given future GhGs (Appendix Fig. 13).

In summary, future GhGs are associated with significantly less frequent TCs in the Northwestern Pacific and in the Southern Indian Ocean, and more frequent TCs over the North Atlantic. These results are maintained when we

Table 3 Ensemble mean number of TCs/year in each experiment by ocean basin: North Atlantic (NA), Northeast Pacific (NEP), North Indian (NI), Northwest Pacific (NWP), South Atlantic (SA), Southeastern Pacific (SEP), Southern Indian (SI), Southwestern Pacific (SWP)

	CTLhist	ghgHaerF	ghgFaerH	CTLfut
NA	17.3[all]	12.9[all]	27.0[all]	21.0[all]
NEP	28.7[b,d]	18.3[a,c]	28.4[b,d]	19.7[a,c]
NI	7.6[d]	7.3[d]	9.3	11.0[a,b]
NWP	25.8[b,c]	30.6[a,c]	19.9[all]	28.4[c]
SA	1.4[c,d]	1.9[d]	2.8[a]	3.9[a,b]
SEP	2.0[b]	3.5[a]	2.4	2.3
SI	16.1[all]	12.9[all]	8.2[a,b]	9.7[a,b]
SWP	16.2[c]	17.0[c]	12.3[a,b]	15.3

For each basin, the values that are significantly different from each other at or above the 95% confidence level are represented by a superscript, with [a] representing values significantly different from CTLhist; [b] from ghgHaerF; [c] from ghgFaerH; and [d] from CTLfut. When the values are significantly different from all the others, it is marked with [all]

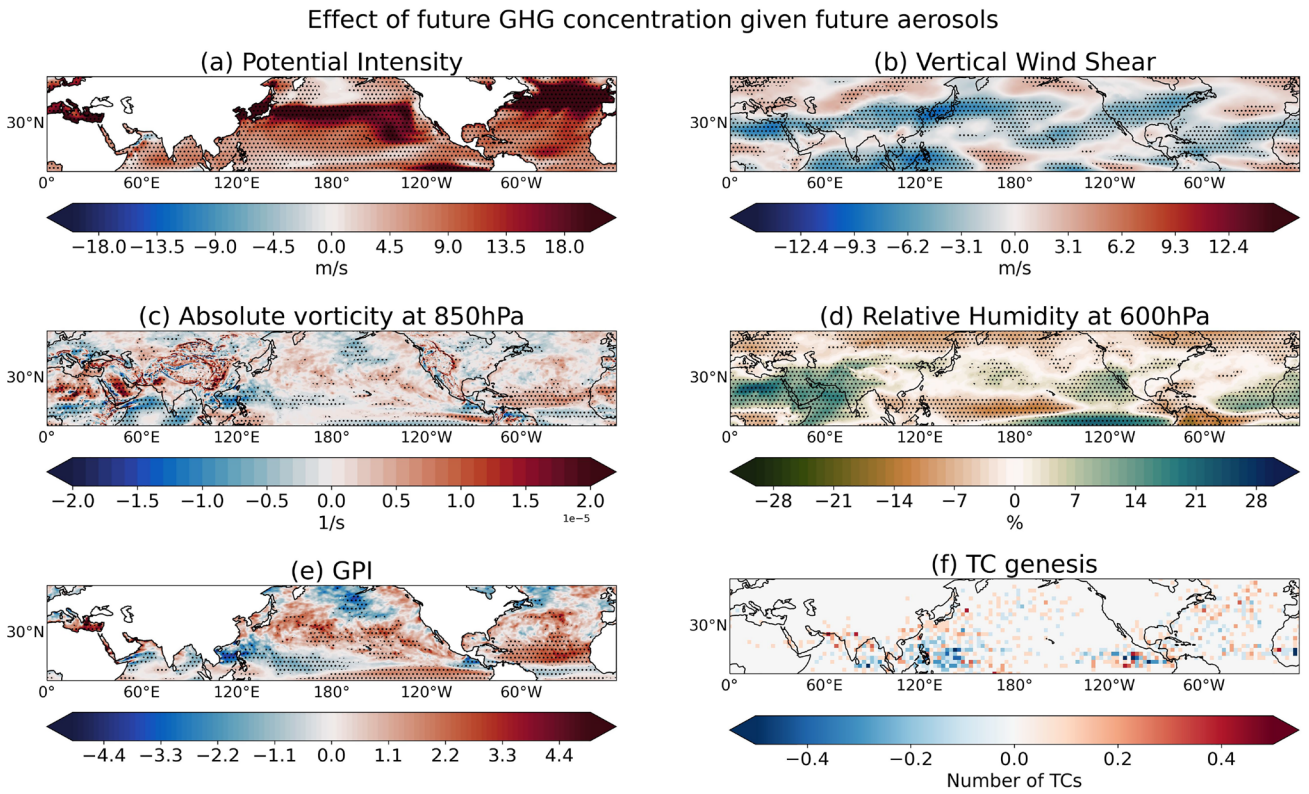

Fig. 4 Difference between the ASO-averaged, ensemble-mean of the CTLfut minus ghgHaerF experiments (representative of the effect of the future change in GhGs given future aerosols) for **a** potential intensity (m/s); **b** vertical wind shear between 850 and 200 hPa (m/s); **c** absolute vorticity at 850 hPa (s^{-1}), **d** relative humidity at 600 hPa (%), **e** GPI (dimensionless), and **f** TC genesis in a 2.5° grid (number of TCs). Stippling indicates significant anomalies at or above the 95% significance level for panels (a–e). Values are shown for the Northern Hemisphere

consider only TCs generated in the tropics (Table 7). These regional changes compensate each other, and result in no significant changes in global TC number. The percentage of intense TCs significantly increases due to future GhGs, leading to increases in seasonal ACE (Sect. 3.1).

3.3 Response in regional tropical cyclone activity to the atmospheric effects of future aerosols

The significant TC responses to the atmospheric effect of the decline in aerosols emissions in the future are concentrated in the Northern Hemisphere (Fig. 3 and Table 3), with fewer TCs in the North Atlantic (− 4.4 and − 6.0 TCs/year for ghgHaerF minus CTLhist and CTLfut minus ghgFaerF, respectively) and in the Northeast Pacific (− 10.4 and − 8.7 TCs/year for ghgHaerF minus CTLhist and CTLfut minus ghgFaerF, respectively). Meanwhile, TCs become more frequent in the Northwest Pacific (+ 4.8 and + 8.5 TCs/year for ghgHaerF minus CTLhist and CTLfut minus ghgFaerF, respectively).

Changes in the South Asian Monsoon associated with the atmospheric effect of future aerosols can help explain the changes in environmental variables related to tropical cyclogenesis in the Northwest Pacific. Monsoon activity is one of the factors that modulates TC frequency in the Northwest Pacific, with more intense summer monsoon activity leading to more frequent TCs (Weng et al. 2022); approximately 73% of the July–November Northwest Pacific TCs are formed within the monsoon trough (Molinari and Vollaro 2013). In CMIP6, the monsoon precipitation over land is projected to increase by the end of the 21st century, in both the SSP2-4.5 Jin et al. 2020; Chen et al. 2020, and in the SSP5-8.5 pathways (Moon and Ha 2020; Chen et al. 2020; Shekhar et al. 2024). We found a similar pattern when considering only the atmospheric effect of the reduction in aerosols. There is an increase in background precipitation over South Asia, stretching to the Northwest Pacific, and a reduction in background rainfall in the North Indian Ocean associated with the atmospheric effect of the reductions in aerosols. Accompanied by reductions in the sea level pressure over the continent and stronger monsoon westerlies over the continent, this pattern suggests an intensification of the summer South Asian monsoon (Fig. 5h). This generates greater ascent and greater relative humidity

at the mid-levels over the Northwest Pacific (Fig. 5d-f), and contributes to a weakening of the trade winds around the Northwest Pacific (Fig. 5g), increasing absolute vorticity closer to the continental areas (Fig. 5c). Together, these responses contribute to a more favorable environment for TC development, reflected in increases in GPI (Fig. 5e) and DGPI (Fig. 12c) in the area, and in the greater TC genesis near the Philippines (Fig. 5i). Because these are not coupled atmosphere-ocean experiments, they exclude an important mechanism by which aerosols likely influence the monsoons. The simulated pattern of change is, however, consistent with studies that suggest that increases in anthropogenic aerosol concentrations are associated with a weakening of the summer monsoon in the historical period (Saha and Ghosh 2019; Guo et al. 2015). The response of the monsoon to the atmospheric effect of future aerosols given historical GhGs (shown in Fig. 5) is consistent with the responses found for the effect of aerosols given future GhGs (Appendix Fig. 14).

While there is a statistically significant reduction of TC frequency in the North Atlantic due to future aerosols given

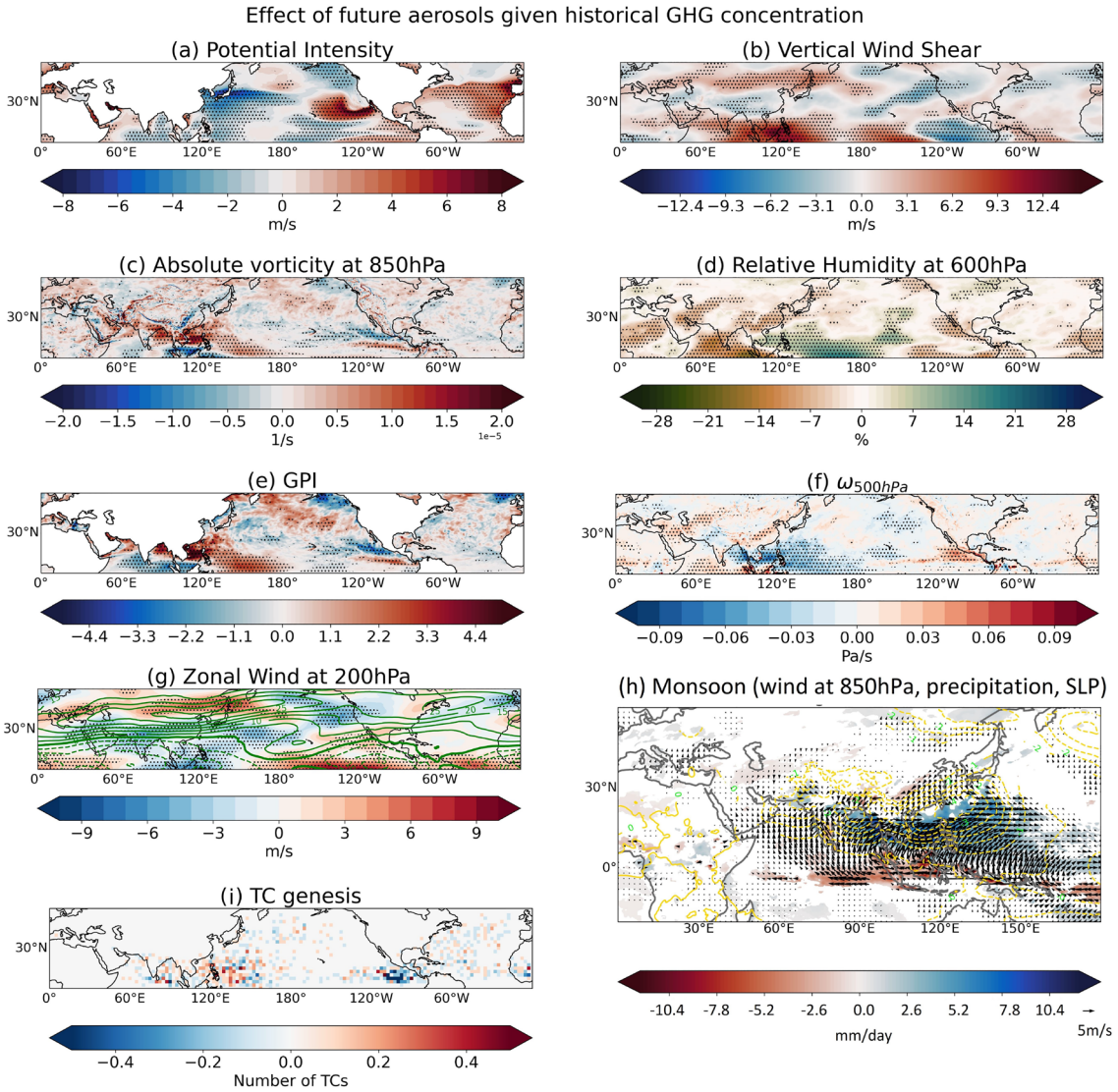

Fig. 5 Difference between the ASO-averaged, ensemble-mean of the ghgHaerF minus CTLhist experiments (representative of the atmospheric effects of future aerosol given historical GhG) for **a** potential intensity (m/s); **b** vertical wind shear between 850 and 200 hPa (m/s); **c** absolute vorticity at 850 hPa (s^{-1}) and **d** relative humidity at 600 hPa (%); **e** genesis potential index (GPI, dimensionless); **f** Pressure vertical velocity (omega) at 500 hPa (Pa/s); **g** zonal wind at 200 hPa (m/s). Contours in this panel shows the ensemble mean zonal wind at 200 hPa in the CTLhist experiment; **h** Sea level pressure (contour), precipitation (colors) and 850- hPa wind; **i** TC genesis in a 2.5° grid (number of TCs). For panels (**a**–**g**), stippling indicates significant anomalies at or above the 95% significance level. In panel (**h**), the values are only shown for the Northern Indian and Northwestern Pacific to focus on the anomalies related to the monsoon, and only significant values are shown

both historical and future GhGs, there are no significant responses in GPI, potential intensity, absolute vorticity, mid-level humidity, vertical velocity, or DGPI (Figs. 5a–f and 12c) to future aerosols that could explain these responses, and there is only a weak increase in vertical wind shear in the tropical North Atlantic and Gulf of Mexico. Neither of these changes can explain the reduction in TCs in the North Atlantic, that is widespread through the ocean basin (Fig 5i).

Meanwhile, there is an overall reduction in GPI over the Northeast Pacific (Fig. 5e), associated with an anticyclonic anomaly in the absolute vorticity (Fig. 5c) due to future aerosols. Under historical GhGs, this is associated with mid-level drying off the coast of Mexico (Fig. 5d) and anomalous subsidence in the area (Fig. 5f). Together, these patterns contribute to an environment less favorable for TCs (Figs. 5e and 12c), leading to reduced TC genesis in the region (Fig. 5i). Note that there is a reduction in vertical wind shear off the coast of Panama and an increase in vertical wind shear off the coast of Mexico due to future aerosols given historical and future GhGs (Fig. 5b). This could be potentially attributable to a significant weakening of the subtropical jet stream and the upper-level winds over the tropical Northeast Pacific (Fig. 5g). Note that, as local reductions in aerosol emissions are small, the reduction in TC frequency over the Northeastern Pacific is mostly attributed to changes in the large-scale circulation due to remote changes in aerosol emissions, notably over the Northwestern Pacific.

In summary, the atmospheric effect of future aerosol reductions is associated with fewer TCs in the North Atlantic and the Northeast Pacific, while they become more frequent in the Northwest Pacific. The frequency changes over the North Atlantic and Northwest Pacific are of the opposite sign of the ones found due to increasing GhGs alone (Sect. 3.2). These results are maintained when only TCs formed over the tropics and subtropics are considered (Table 7). This suggests that the atmospheric effect of future aerosols mitigates the TC frequency changes due to the increase in GhG concentrations. The total global TC frequency does not significantly change due to the atmospheric effect of future aerosols, and neither does the total number of TCs in the Northern Hemisphere. There is only a small, but significant reduction in the number of TCs in the Southern Hemisphere due to future aerosols given historical GhGs, associated with a significant reduction in TC frequency in the South Indian Ocean in this experiment. As no significant changes were found given future GhGs, neither at the 95% nor at the 90% confidence level, we chose not to explore these responses further. The changes in seasonal ACE due to future aerosols are either insignificant or characterized by a small reduction, and we did not find any significant changes in the latitude of the maximum wind speed in either hemisphere due to future aerosols (Appendix Fig. 15). On the other hand, the atmospheric effect of future aerosols significantly contributes to TC intensification, as the fraction of major TCs increases in both GhGs scenarios, compounding to the effect of GhGs (Sect. 3.1).

3.4 Response in regional tropical cyclone activity to future greenhouse gases and aerosols in combination

The overall change in TC frequency in these experiments is affected by both the atmospheric effects of future aerosols and by GhGs (including through GhG effects on SST). In the Northeast Pacific, the total response of TC frequency is dominated by the aerosol effects, with a significant reduction of − 9.0 TCs/year in the CTLfut minus the CTLhist experiments (Fig. 3b, see also Table 3). This is associated with significant reduction in the GPI off the coast of Mexico and Panama (Fig. 6e), related to significant reductions in relative humidity at 600 hPa (Fig. 6d), and significant negative anomalies in absolute vorticity over off the coast in the Northeast Pacific (Fig. 6c), leading to an environment less favorable to TC genesis (Fig. 6f). This counteracts the effect of the increase in the potential intensity over the Northern Hemisphere (Fig. 6a), and the significant weakening of the vertical wind shear over the basin (Fig. 6b).

Meanwhile, TCs are projected to become significantly more frequent in the North Atlantic by + 3.7 TCs/year (Fig. 3c), a more modest increase than the expected changes without the contribution of future changes in aerosol concentrations. These changes were analyzed by Sena et al. (2022) and are associated with increases in SST, reduced vertical wind shear, and a moister atmosphere in the mid-levels (see also Fig. 6). A positive anomaly of absolute vorticity also contributed to the response (Fig. 6c). In the Indian Ocean, TCs become significantly more frequent in the North Indian Ocean (+ 3.4 TCs/year) and less frequent in the South Indian Ocean (− 6.4 TCs/year) (Fig. 3d–f). The reductions in TC frequency in the Southern Indian Ocean are associated with an increase in vertical wind shear in JFM, associated with mid-level drying over the western and central Southern Indian Ocean, leading to a decrease in GPI over large portions of the tropics, including the northwestern coast of Australia (Appendix Fig. 15). No significant changes in TC frequency were found in the Northwest Pacific when considering the combined effect of both aerosols and GhGs (Fig. 3a).

In summary, the total response of global TC frequency to the effect of both future aerosols and GhGs is related to increases in TC frequency in the North Atlantic and the North Indian Ocean, while TCs become less frequent in the South Indian Ocean and in the Northeast Pacific. These changes compensate each other, and no significant changes are found either in the global TC frequency or over both hemispheres separately (see Sect. 3.1). The latitude of the

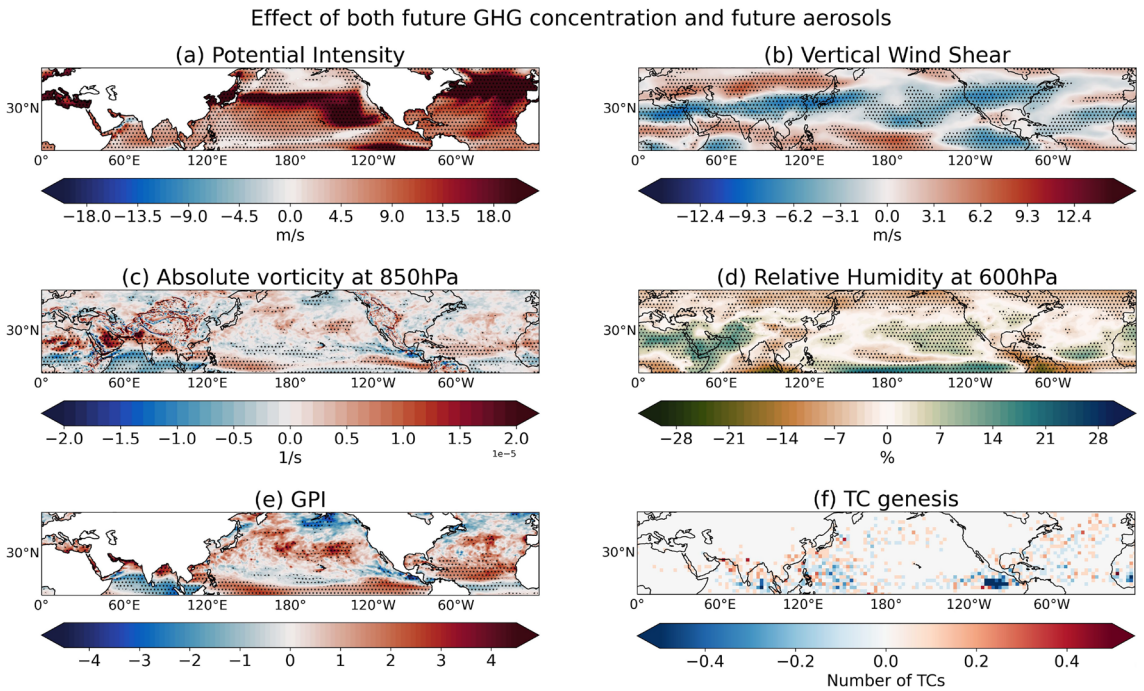

Fig. 6 Difference between the ASO-averaged, ensemble-mean of the CTLfut minus CTLhist experiments (representative of the effect of the changes in both GhGs and aerosols) for **a** potential intensity (m/s); **b** vertical wind shear between 850 and 200 hPa (m/s); **c** absolute vorticity at 850 hPa (s^{-1}), **d** relative humidity at 600 hPa (%), **e** GPI (dimensionless), and **f** TC genesis in a 2.5° grid (number of TCs). Stippling indicates significant anomalies at or above the 95% significance level for panels (**a**–**e**)

maximum wind speed significantly moves poleward in both hemispheres, as a consequence of the increase in GhGs (Appendix Fig. 16). The number of major TCs increases with the concurrent changes in aerosols and GhGs, leading to a greater response than due to either aerosols or GhGs alone. The seasonal ACE increases as a consequence of the increase in the percentage of major TCs. The magnitude of the change in TC intensity, as well as the changes in regional TC frequency, suggest that both future GhGs and future aerosols contribute to the responses in TC activity in the CTLfut minus CTLhist experiments.

3.5 Tropical cyclone precipitation

The model simulations project an increase in TC precipitation in the future compared to the historical period for joint changes in GhGs and aerosols (CTLfut-CTLhist) (Fig. 7a). Total TCP increases by about 14.1 ± 2.1%/K, or 52.8 ± 3.7%, globally due to the effect of both the reduction in aerosol emissions and the increase in GhG concentrations (Fig. 7a and Table 4). GhG changes account for an increase of 6.9 ± 1.2%/K, or 28.1 ± 3.6%, given historical aerosols (ghgFaerH minus CTLhist) and 8.3 ± 1.4%/K, or 33.3 ± 4.0%, given future aerosols (CTLfut minus ghgHaerF). The rate of change of TCP per degree of SST warming with GhGs is similar to the default expectation of 7%/K that would be obtained by the Clausius–Clapeyron relation alone (e.g. Knutson et al. 2020). Meanwhile, the percent change of TCP is significantly greater than the global increase in precipitation of 8.20 ± 0.67% and 8.11 ± 0.55% for historical and future aerosols, respectively, and 13.25 ± 0.62% for both future GhGs and future aerosols (Appendix Table 8). The mean and uncertainty of the global precipitation is defined as the difference between the 10-member ensemble mean in each experiment and its 95% confidence interval, respectively. While extreme precipitation is expected to increase by the Clausius–Clapeyron rate, the mean global precipitation increases are more modest, ranging from 1 to 2%/K in most CMIP5 climate models (Giorgi et al. 2019). Thus, the global mean precipitation response found in the CTLfut minus CTLhist experiments has a similar range, with a global mean change in SST in the simulations of 6 °C, in regions equatorward of 60° of latitude. In regions equatorward of 40° of latitude, the global change in precipitation is about 10.6% and SST warms by about 5.2 °C, leading to a similar rate of warming.

Regionally, the greatest difference between the rate of change in TC precipitation due to both aerosols and GhGs than due to GhGs alone is found in the Northwest Pacific. Over this region, there is an increase in of 17.1 ± 4.0%/K in total TCP for CTLfut-CTLhist compared to 3.6 ± 2.6%/K and 5.8 ± 2.5%/K for changes in GhGs given future and

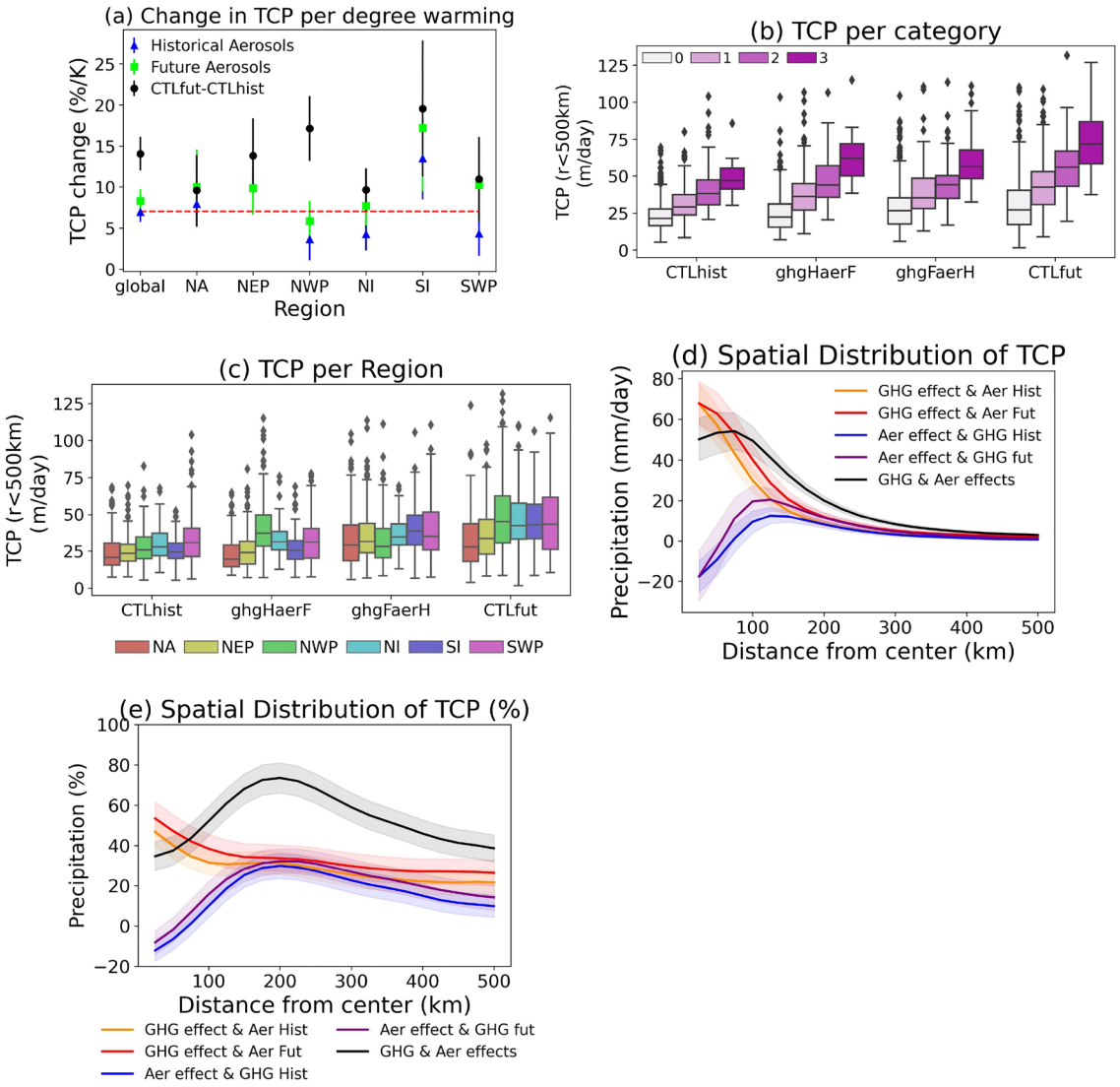

Fig. 7 **a** Rate of change in total TC precipitation per degree Celsius of warming. The points represent the mean change due to GhGs given constant historical aerosols (ghgFaerH minus CTLhist, in blue triangle), given constant future aerosols (CTLfut minus ghgHaerF, green square) and varying both aerosols and GhGs (CTLfut minus CTLhist, black circle). The changes are calculated for the all TCs (global) and in each basin. Error bars represent the 95% confidence interval. The value of 7%/K is marked by a red line. **b** Boxplot of the mean TCP in each experiment, divided by categories according to the Saffir–Simpson scale for total TCP, within 500 km from the center of the TC (in m/day, or 10^3 mm/day). **c** Boxplot of the mean TCP for each region, divided by experiments measured as the total TCP within 500 km from the center of the TC (in m/day, or 10^3 mm/day). **d** Mean response of rainfall (mm/day) around TC the relative to the distance from the center of the TCs for: ghgFaerH minus CTLhist (in orange), CTLfut minus ghgHaerF (red), ghgHaerF minus CTLhist (blue), CTLfut minus ghgFaerH (purple), and CTLfut minus CTLhist (black). Shading represents the 95% confidence level. **e** Same as **d**, but with the response represented in percentage. For panels **b**, **c**, the boxplot represents the internal variability of the experiments for all TCs in the 10 ensemble members in each experiment. The edges of the boxplots show the 25th and 75th percentiles. Whiskers represent 1.5 the interquartile range. The median is marked as a straight line

historical aerosol concentrations, respectively. Changes in aerosol emissions can help explain this response.

We found a significant increase in TCP associated with the atmospheric effect of the reduction in aerosol emissions (Table 5). Globally, the model projected an increase of 52.8 ± 3.7% in total TCP due to both future aerosols and GhG changes. Experiments with only a reduction in aerosol emissions produced TCP increases of 14.7 ± 3.9% given historical GhGs (ghgHaerF minus CTLhist) and 19.3 ± 4.1% given future GhGs (CTLfut minus ghgFaerH). These values exceed the mean increase in global precipitation in the model (4.75 ± 0.77 and 4.67 ± 0.38 % for historical and future GhGs, respectively; Appendix Table 8). Regionally, there were little significant changes, as the signal is weak

Table 4 Percent change in total TC precipitation per degree Celsius of change in SST at the area of formation of the TCs

	Effect of the future GhGs					
	Given historical aerosols		Given future aerosols		CTLfut–CTLhist	
	Mean (%/K)	Error (%/K)	Mean (%/K)	Error (%/K)	Mean (%/K)	Error (%/K)
Global	6.9	1.2	8.3	1.4	14.1	2.1
NA	7.9	2.8	10.0	4.6	9.6	4.3
NEP	9.9	2.4	9.9	3.3	13.8	4.5
NWP	3.6	2.6	5.8	2.5	17.1	4.0
NI	4.2	2.0	7.7	2.4	9.6	2.6
SI	13.5	5.0	17.2	7.8	19.5	8.3
SWP	4.3	2.7	10.2	4.0	10.9	5.2

The response is due to future GhGs given historical aerosols (difference between the ghgFaerH minus the CTLhist experiment) and given future aerosols (CTLfut and ghgHaerF), and due to future changes in both GhGs and aerosols (CTLfut minus CTLhist). The values are shown for all TCs (global) and for each basin. The error corresponds to deviations from the mean under the 95% confidence interval

Table 5 Percent change in total TC precipitation ($r < 500$ km) due to future aerosols, and difference in SO_2 concentration integrated in the column (in ppt mol of SO_2/mol of dry air and in percentage) at the area of formation of the TC

	Atmospheric effect of future aerosols			
	Given Historical GhGs (ghgHaerF–CTLhist)			
	Total TCP (%)	Error (%)	SO_2 (ppt)	Error (ppt)
Global	14.7	3.9	− 15.0 (− 30%)	6.6
NA	− 2.2	12.0	− 16.7 (− 38%)	7.7
NEP	2.7	8.3	2.6 (+ 3%)	20.5
NWP	44.1	6.2	− 9.2 (− 25%)	9.8
NI	7.1	12.1	− 108.0 (− 79%)	44.4
SI	6.0	9.1	− 2.9 (− 14%)	4.2
SWP	− 3.5	11.1	2.2 (+ 9%)	11.7
	Given future GhGs (CTLfut–ghgFaerH)			
	Total TCP (%)	Error (%)	SO_2 (ppt)	Error (ppt)
Global	19.3	4.1	− 38.0 (− 46%)	11.8
NA	− 1.0	10.4	− 21.4 (− 39%)	8.9
NEP	4.7	8.9	− 3.0 (− 4%)	19.6
NWP	53.3	7.6	− 91.6 (− 62%)	48.9
NI	25.1	9.8	− 146.0 (− 73%)	55.2
SI	11.0	12.6	− 22.5 (− 58%)	11.2
SWP	13.8	11.6	− 2.0 (− 7%)	11.5
	CTLfut-CTLhist			
	Total TCP (%)	Error (%)	SO_2 (ppt)	Error (ppt)
Global	52.8	3.7	− 4.8 (− 10%)	6.8
NA	34.8	9.7	− 10.5 (− 24%)	8.3
NEP	46.7	7.7	− 6.7 (− 9%)	19.6
NWP	73.4	6.7	18.1 (− 49%)	13.5
NI	52.8	10.3	− 80.3 (− 59%)	44.9
SI	75.1	9.7	− 3.7 (− 18%)	3.1
SWP	36.6	10.3	0.7 (− 3%)	11.3

The response due to the atmospheric effect of future aerosols is shown given historical GhGs (difference between the ghgHaerF minus the CTLhist) and given future GhGs (CTLfut and ghgFaerH), and for changes in both GhGs and aerosols (CTLfut minus CTLhist). The values are shown for all TCs (global) and for each basin. The margin of error corresponds to deviations from the mean under the 95% confidence interval

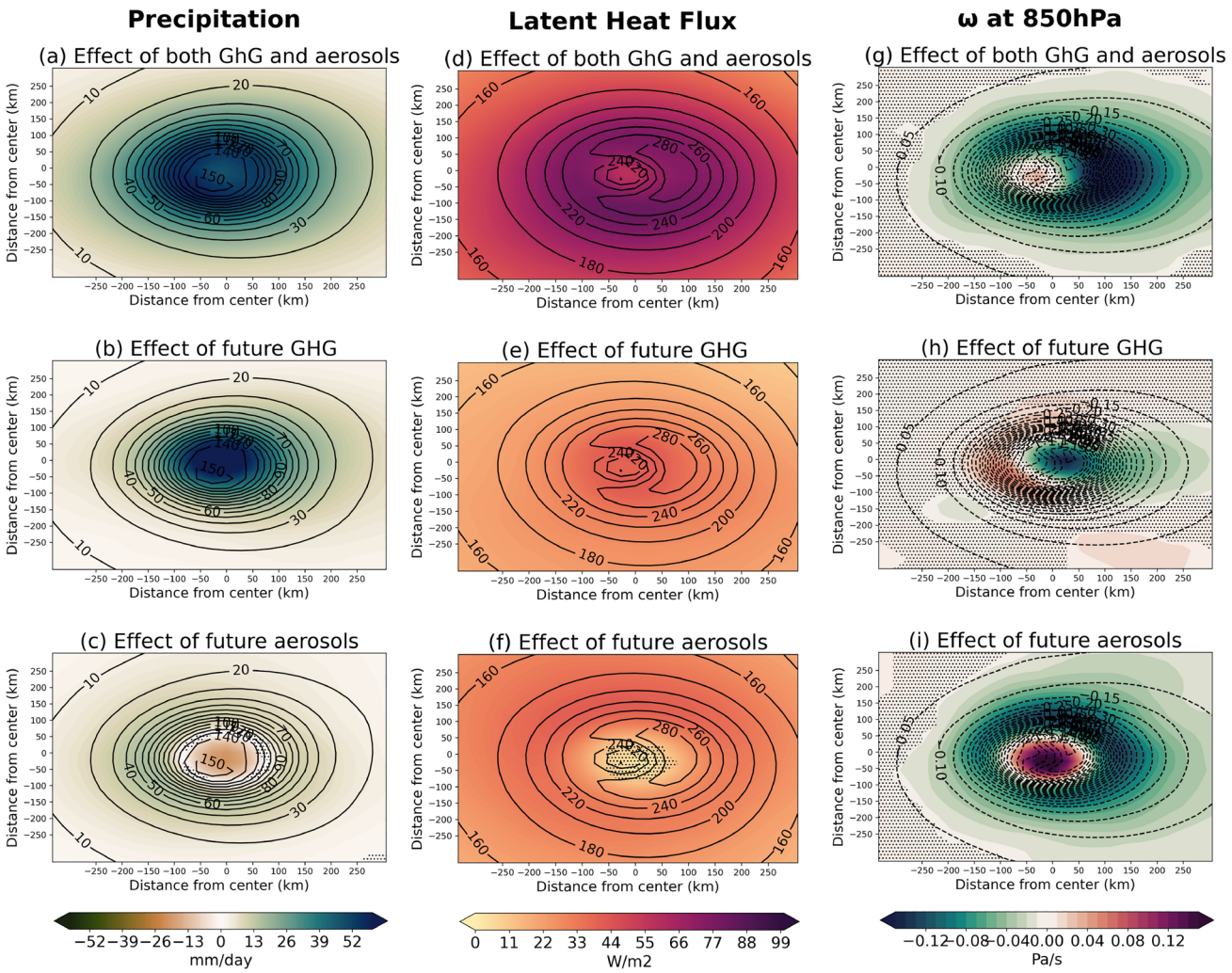

Fig. 8 Difference between the mean precipitation within a 300 km radius of the TCs for **a** CTLfut minus CTLhist experiments, representative of the effect of both future aerosols and future GhGs (colors), and mean values in the CTLhist experiment (contours); **b** ghgFaerH minus CTLhist experiments (colors), representative of the effect of future GhGs given historical aerosols, and mean values in the ghgHaerF experiment (contours); **c** ghgHaerF minus CTLhist, representative of the atmospheric effect of the future aerosols given historical GhGs (colors), and mean values in the CTLhist experiment (contours); **d–f** Same as **a–c**, but for Surface Latent Heat Flux (W/m^2); **g–i** Same as **a–c**, but for vertical velocity in pressure coordinates (Pa/s) at 850 hPa. Stippling represents areas where the differences are not significant at the 95% confidence level

relative to the noise from the ensemble members, with the exception of a significant increase in total TCP over the Northwest Pacific given future aerosols, of 44.1 ± 6.2% and 53.3 ± 7.6% given historical and future GhGs.

More intense TCs have been suggested as a factor in the increase in TCP (Liu et al. 2019). As discussed in Sect. 3.1, TCs become more intense due to both future GhGs and aerosols (see also Fig. 2). In our experiments, stronger TCs are generally associated with higher total TCP (Fig. 7b). However, the relation between TCP and TC intensity is weakened with distance from the center of the TC, and is insignificant in its outer-bands (Appendix Fig. 17). Meanwhile, similar values to the total TCP changes due to future aerosols are found both in areas where there is a significant influence of intensity on TCP, such as TCP100 km, and over areas where intensity is not significantly associated with TCP, such as TCP500 km (Appendix Table 9). This implies that, although there is a correlation between TC strengthening and the overall increase in total TCP, this relationship is driven by its impact on inner-core TCP. Conversely, the wetting simulated in the outer-band cannot be attributed to more intense TCs. This distinction is crucial, considering that the wetting in total TCP due to the atmospheric effects of future aerosols is linked specifically to outer-band wetting, while TCP is reduced in the inner-core (see Appendix Table 9, Fig. 7d).

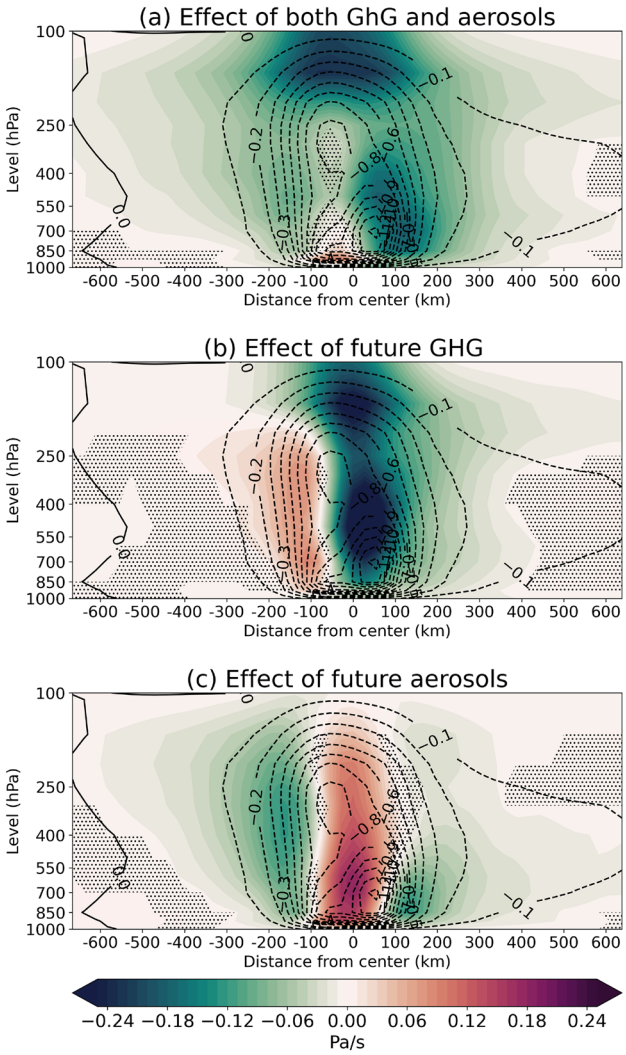

Fig. 9 Vertical profile of the ensemble-mean latitudinal-averaged cross-section of the mean vertical velocity within a 600 km radius of the TCs for: **a** CTLfut minus CTLhist experiments, representative of the effect of changing both aerosols and GhG/SST (colors), and mean values in the CTLhist experiment (contours); **b** CTLfut minus ghgHaerF experiments (colors), representative of the effect of future GhGs given historical aerosols, and mean values in the ghgHaerF experiment (contours); **c** ghgHaerF minus CTLhist, representative of the atmospheric effect of the future aerosols given historical GhGs (colors), and mean values in the CTLhist experiment (contours). Stippling represents areas where the differences are not significant at the 95% confidence level

Therefore, future strengthening of TCs alone cannot fully account for the increased TCP identified in this study.

We also explored the possibility that the changes in global TCP are partially due to the regional changes in TC frequency. As described in Sect. 3.3, the atmospheric effects of future aerosols are associated with less frequent TCs in the North Atlantic and Northeast Pacific, and more frequent TCs in the Northwest Pacific. There are generally small, mostly insignificant, differences in the TCP depending on the region of occurrence of the TC (Fig. 7c). Note, however, that in both experiments with future aerosols (ghgHaerF and CTLfut) TCP in the Northwest Pacific is significantly greater than in the North Atlantic and Northeast Pacific (Fig. 7c). The Northwest Pacific also has consistently the greatest value of area-averaged summer precipitation in all experiments, though this difference is only significant for the ghgHaerF and CTLfut experiments. Moreover, the Northwest Pacific has the greatest basinwide change in precipitation unrelated to TCs due to future aerosols, with an increase of 27.7 ± 4.7% and 35.1 ± 7.3% in precipitation during ASO, given historical and future GhGs, respectively. Meanwhile, no significant changes in background precipitation were found over the Northeast Pacific and the North Atlantic due to the atmospheric effects of aerosols (Appendix Table 10). We found a significant, positive correlation between the mean summer area-averaged precipitation in a basin and the mean TCP in that basin ($r = 0.5$, $p = 0.011$). It is possible that the increase in the fraction of TCs occurring over the Northwest Pacific, where the greatest absolute values of area-averaged precipitation and the greatest increase in area-averaged precipitation occur, skews the global TCP towards greater values with future aerosols. Still, the changes in background precipitation over the Northwest Pacific are smaller than the TCP increase in the Northwest Pacific (44.1 ± 6.1% and 53.3 ± 7.3%, Table 5 and Appendix Table 10).

While both future changes in GhGs and aerosols contribute to an increase in TCP, there are differences in how each of these factors contribute to the spatial distribution of this response. TC responses to GhGs are characterized by greater increases in rainfall at the center of the TC, and this rainfall increase is reduced with distance from the TC center (Figs. 7d, e and 8b). Meanwhile, the atmospheric response to future aerosol emissions causes a reduction in TCP near the center of the TC and more rainfall at its outer-bands (Figs. 7d, e and 8c). The response to both changes in GhGs and aerosols jointly shows signs of the contributions of both of these changes, with more modest precipitation enhancements at the center of the TC and greater precipitation increases at its outer-bands than what would be expected from GhG changes alone (Fig. 7d, e). The highest increase in TCP in CTLfut relative to CTLhist, when expressed as a percentage, is simulated at approximately 200 km away from the center of the TC. This location coincides with where the greatest enhancement in TCP due to aerosols is simulated (Fig. 7e).

Differences in the structure of the energy flux responses in the TCs may help explain the differences in the spatial structure of the TCP response to future GhGs and future aerosols. The cleaner aerosol state is associated with an overall increase in surface latent heat flux, which is stronger at distances greater than 100 km from the center of the TC

than near its center (Fig. 8f and Appendix Fig. 18f). This generates a more unstable environment further from the TC center, leading to more ascent in the area and greater compensating subsidence at the inner-core of the TC. (Fig. 8i and Appendix Fig. 18i). This pattern of stronger ascending motion at the outer-band and greater subsidence in the TC inner-core is not confined to the lower-levels, and expands throughout the troposphere up to 100 hPa (Fig. 9c). One possible mechanism for these changes is that the lower aerosol concentration leads to a lower number of cloud condensation nuclei (CCN). While the microphysical effects of the changes in aerosol concentration are not represented in E3SM, there are macrophysical effects of the changes in the distribution of size and quantity of CCNs. Under fixed SSTs, a similar amount of moisture available for cloud formation is divided into a smaller number of CCNs which, in our experiments, results in a quicker and more intense development of rainfall in the rainbands. This, in turn, reinforces the eyewall, leading to more subsidence in the inner-core of the TC.

Future GhGs also increase evaporation and surface latent heat flux. However, the largest increases in surface latent heat are found at the center of the TC (Fig. 8e and Appendix Fig. 18e). The increase in surface latent heat due to future GhGs is expected due to the increase in SST, leading to increased evaporation. This leads to a more unstable environment at the inner-core of the TC than at its outer-band, and to stronger ascending motion at the inner-core of the TC than at its outer-bands (Fig. 8h and Appendix Fig. 18h), thus favoring convection near the inner-core. This stronger ascending motion at the center of the TC is found throughout the column, and it is accompanied by areas where there is a reduction in vertical velocity at the west of the TC center (Fig. 9b). While this subsidence appears in both of the responses due to GhGs with historical and future aerosols and its effect can also be seen in the CTLfut minus CTLhist responses, it is not clear why the subsidence appears consistently at east of the TC.

The total changes in the TC structure point to contributions from both the future changes in aerosols and GhGs. Surface latent heat flux increases in the whole area of the TC, though the increases are weaker at the center of the TC (Fig. 8d). There is greater ascent at the lower-levels at a 100–300 km radius of the TC due to combined future GhGs and aerosols than either due to future aerosols or future GhGs alone, though this increase is asymmetrical, with smaller increases at the western portions of the TC in similar areas where the anomalous subsidence is found due to future GhGs (Fig. 8g). Meanwhile, there is an anomalous subsidence at 850 hPa over areas closer than 50 km from the center of the TC, though not as strong as that found in the cleaner aerosol state alone (Fig. 8g). However, unlike the pattern due to the atmospheric effect of future aerosols, this anomalous subsidence at the center of the TC is confined to the lower-troposphere. The vertical cross-section of the TC suggest a stronger increase in ascent over areas between 100–200 km from the center of the TC, consistently throughout the column (Fig. 9a). Meanwhile, there are no significant changes in vertical velocity closer to the TC center between 850 hPa and 250 hPa, and ascending motion is favored above 250 hPa (Fig. 9a), similar to the anomalies found at this altitude due to GhGs alone. Finally, the pattern of the TCP changes indicates the contribution of both factors, with an increase in precipitation over the entire extent of the TC but a more modest increase closer to the center of the TC than what is found due to future GhGs alone (Fig. 8a).

4 Discussion and conclusions

Although future changes in aerosols and GhGs are commonly analyzed together in climate models, reductions in aerosol emissions and increases in GhG concentrations have had opposite effects on TC frequency and/or intensity in the historical climate according to some models (e.g. Sobel et al. 2016, 2019; Ting et al. 2015; Mann and Emanuel 2006; Dunstone et al. 2013; Booth et al. 2012). While aerosols can modulate TC activity by cooling SSTs, thereby reducing TC potential intensity, here we focus on the atmospheric effect of the decline of aerosol emissions under fixed SSTs, using TC-resolving Earth system model (E3SM) simulations under the SSP5-8.5 scenario for the late-21st century.

We found that the future increases in GhGs and the atmospheric effect of decreases in aerosols combined lead to more frequent TCs in the North Atlantic (21%) due to increased PI, reduced vertical wind shear, and a moister mid-troposphere. In the South Indian Ocean, the combined forcing results in 40% fewer TCs due in part to increased vertical wind shear and mid-level drying. In the Northeast Pacific there is a reduction of 31% in TC frequency, due to mid-level drying and a reduction in low-level absolute vorticity. The regional TC responses to increased GhGs are partially compensated by the atmospheric effect of future aerosols. In particular, future GhGs (aerosols) lead to more (less) frequent Atlantic TCs and less (more) frequent Northwest Pacific TCs. Notably, these regional TC changes compensate each other, producing insignificant changes in global TC frequency in response to the atmospheric effects of future aerosols and future GhGs individually and in combination.

Alone, the atmospheric effect of a cleaner atmosphere is associated with a more active monsoon season over South Asia. Accordingly, the atmosphere over the Northwest Pacific becomes more moist and anomalies in the trade winds lead to reductions in vertical wind shear and increases in low-level absolute vorticity, supporting a more favorable TC environment over the Northwest Pacific. Note that as the experiments used prescribed SSTs, this monsoon

enhancement may be more intense than in a coupled atmosphere-ocean model. Still, it is consistent with studies that suggest that anthropogenic aerosols are associated with a weakening of the summer monsoon, while GhGs contribute to a strengthening of the monsoon in the historical period (Saha and Ghosh 2019; Guo et al. 2015).

In addition, the varied regional TC frequency responses due to the atmospheric effects of future aerosols indicate that the changes in TC frequency identified in this study predominantly stem from the impact of the alterations in aerosol concentration and distribution on the large-scale atmospheric circulation, similar to the dynamic pathway identified by Murakami et al. (2020). Despite insignificant effects on global TC frequency, both the atmospheric effect of reduced aerosols and increased GhGs contribute to stronger TCs in the future. The number of major TCs increases significantly in the future climate due to combined GhG and aerosol forcings, with an increase that is greater than the individual contribution of reduced aerosols and increased GhGs.

TC precipitation is also significantly affected by both the atmospheric effect of reduced aerosols and increased GhGs. Global TCP increases by $52.8 \pm 3.7\%$ (Table 5), or $14.1 \pm 2.1\%/\,^{\circ}\mathrm{C}$ (Table 4), which is greater than the theoretical $7\%/^{\circ}\mathrm{C}$ increase estimated by Clausius–Clapeyron. Future GhGs alone contribute to TCP changes at a rate similar to the theoretical value, with increases of $6.9 \pm 1.2\%/\,^{\circ}\mathrm{C}$ and $8.3 \pm 1.4\%/\,^{\circ}\mathrm{C}$, given historical and future aerosol conditions, respectively. This corresponds to a total increase of $28.1 \pm 3.6\%$ and $33.3 \pm 4.0\%$, respectively. Aerosol reductions have a relatively smaller contribution, with increases of $14.7 \pm 3.9\%$ and $19.3 \pm 4.1\%$ given historical and future GhGs and SSTs, respectively.

While future aerosol and GhG contributions to the TCP response are of the same sign, they have important differences in their spatial distribution. Increased GhGs increase rainfall at the inner-core of the TC. There is greater surface latent heat release and ascent in the TC inner-core, favoring convection. This response fades with distance from the TC center, leading to weaker precipitation increases at the TC outer-bands. On the other hand, future aerosol reductions are associated with precipitation enhancements at the outer-bands of the TC, with greater surface latent heat release and greater ascent in the TC outer-bands, favoring convection. Furthermore, there is anomalous subsidence at the inner-core of the TC due to the atmospheric effect of future aerosols, reducing rainfall in the TC inner-core. The total response to both future aerosols and GhGs/SST jointly is a combination of both of these changes, with greater precipitation increases at the TC outer-bands and weaker precipitation increases at the TC center.

This change in TCP patterns is similar to what has been found in observations. Satellite observations suggest that there is a spatial pattern of TCP trends in the 21st century, with a reduction of precipitation in the TC inner-core and an increase in the outer regions (Guzman and Jiang 2021; Tu et al. 2021). While these studies do not suggest a link to reductions in aerosol concentrations, it is interesting to note that a similar structure was found in this study. Moreover, Lin et al. (2023) found a 11% increase in precipitation within 100 km of the TC center under a 5-fold increase in anthropogenic aerosol concentrations in a cloud resolving model without ocean coupling, with this amount doubling with ocean coupling during the mature stages of the TC. This is consistent the results found in the present study for the reduction in aerosol emissions. Note that Lin et al. (2023) performed the experiments in a convection-permitting model at 3 km horizontal resolution.

In this study, the experiments treat all of the SST change as attributable to GhGs, which is a simplification. Part of the ocean warming could be attributed to the direct effect of the aerosol reductions, which would lead to greater radiative warming of the ocean surface in the future climate. Xu et al. (2018) suggested that 20% of the warming between the historical and late-20th century (2060–2080) RCP8.5 scenario in CESM can be attributed to the future reductions in aerosols, amounting to a 0.6K global warming (0.9K over land). A similar rate was found in the GFDL model, where the reduced aerosol emissions contribute to about 1K global warming by the end of the 21st century in the RCP8.5 scenario relative to the 1881–1920 period, compared to a total warming of nearly 5K (Westervelt et al. 2015). While our experiments with future aerosols neglect this effect due to the experimental design, it is revealing that significant responses in TC activity were found due to future aerosols in basins adjacent to areas with the greatest reductions in aerosol emissions, specifically over the Northwest Pacific.

Note that the experiments analyzed here do not use a coupled ocean. Ocean feedbacks can affect TC development through a few processes, such as: mixing of the surface water with deeper ocean water and cooling the surface, leading to a negative feedback on TC development (Korty et al. 2008; Zhang et al. 2021); increased heat uptake by evaporation (Zhang et al. 2021; Singh and Roxy 2022); and freshening of the upper ocean, leading to cooler underlying SSTs (Schade and Emanuel 1999; Bender and Ginis 2000; Karnauskas et al. 2021; Balaguru et al. 2022; Singh and Roxy 2022). This ocean feedback has also been suggested to enhance precipitation near the eyewall of TCs under high anthropogenic aerosol concentrations, producing more intense TCs than a polluted environment without ocean coupling (Lin et al. 2023). These processes are not represented in atmospheric-only experiments.

As the spatial resolution of these experiments is not sufficient to resolve convection, the results depend on the convection parametrization. This is an important source of uncertainty in the representation of TCs in climate

models, and numerous studies have aimed to understand and improve their representation. A short discussion of this effect can be found in the "Appendix 2".

Aerosol-cloud interaction is still a poorly understood component of the climate system, and it remains a main source of uncertainties in estimations of the radiative feedback in a warming climate (Szopa et al. 2021). This is partially due to scarce observations, with most of the concurrent measurements of profiles of cloud dynamics, microphysics, and aerosols made infrequently or over relatively small areas (Fan et al. 2016). Still, the main source of aerosol influences on the effective radiative forcing under prescribed SST are cloud-mediated effects (Fiedler et al. 2023). The inclusion of a sophisticated parametrization of aerosol-cloud interactions has been shown to improve the zonal mean temperature biases in CMIP5 models (Ekman 2014). While there were significant improvements in CMIP6 models, significant inter-model differences remain. In general, models with a greater positive cloud feedback to GhGs also have a stronger cooling effect from aerosol-cloud interactions, but the magnitude of the aerosol-mediated cloud radiative response to a $4 \times CO_2$ varied from -1.39 to $+0.63$ W/m^2 among 30 CMIP6 models studied by Wang et al. (2021). Even in cloud-resolving models, there is low-confidence in the effect of aerosol-cloud interactions, with bulk schemes unable to fully reproduce the aerosol-cloud interactions, while spectral bin microphysics is both computationally expensive and limited by the observational uncertainties (Fan et al. 2016; Khain et al. 2015).

These possible sources of uncertainty may be reflected in the present study. There is evidence that clouds are highly sensitivity to perturbations in aerosol concentrations in E3SM version 2 (Golaz et al. 2022). The choice of parametrizations may lead to uncertainties in the representation of the indirect effect of the aerosols, as described above. Meanwhile, the representation of microphysics processes associated with cloud formation may lead to further uncertainties, as evidenced by studies that used convection-resolving models which suggest the opposite effect of aerosols on TCP than found in the present study (e.g. Krall and Cottom 2012; Wang et al. 2014; Rosenfeld et al. 2012). This suggests that further research could be performed to address how robust these results are across different climate models and scales.

This research suggests that, while SST may be an important contributor to the TC responses to aerosol emissions, the atmospheric effects of aerosols can significantly contribute to changes in TC activity. Moreover, it highlights the importance of the proper representation of the spatial distribution of aerosols when studying projected changes in future TC frequency and precipitation.

Appendix 1: Supplementary figures and tables

This section includes figures and tables that support the changes in TC frequency and precipitation, discussed in Sect. 4 (Figs. 10, 11, 12, 13, 14, 15, 16, 17, 18) and (Tables 6, 7, 8, 9, 10).

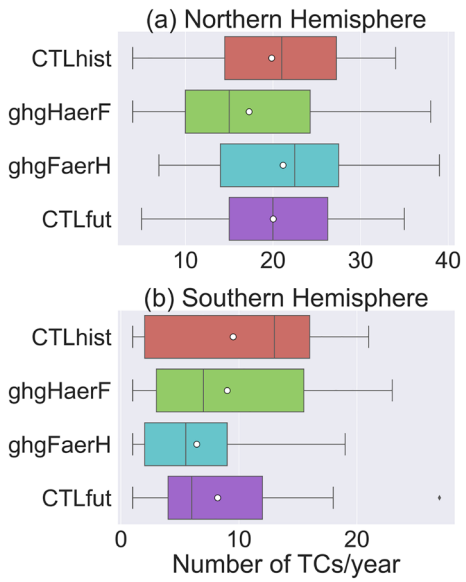

Fig. 10 Total number of TCs in each experiment for **a** the northern hemisphere, and **b** the southern hemisphere. The mean TC frequency in the southern hemisphere for CTLhist and ghgFaerH are significantly different. No other significant changes were found at the 95% level. The boxplot represents the internal atmospheric variability of the 10-member ensemble in each experiment. The edges of the boxplots show the 25th and 75th percentiles. Whiskers represent 1.5 the interquartile range. Outliers are marked with diamond-shaped symbols. The median is marked as a straight line, and the mean is noted by a white circle in panels **a** and **b**

Table 6 Same as Table 2, but considering only TCs formed over 40°S and 40°N

Experiment	Total	cat0	cat1	cat2	cat3	cat4	Major (%)	ACE
CTLhist	89.5[all]	57.9 [all]	23.5[c,d]	7.4 [d]	0.7[c,d]	0	0.8[all]	605.1[b,c]
ghgHaerF	78.3[a]	47.4 [a]	20.9	8.3	1.7[c,d]	0	2.2[all]	525.4[all]
ghgFaerH	79.4[a]	47.5 [a,d]	19.8[a]	7.7 [d]	4.3[all]	0.1	5.5[all]	672.3[a,b]
CTLfut	78.5[a]	41.8 [a,c]	19.0 [a]	10.9 [a,c]	6.6[all]	0.2	8.6 [all]	672.4 [b]

Table 7 Same as Table 3, but considering only TCs formed over 40°*S* and 40°*N*

Experiment	CTLhist	ghgHaerF	ghgFaerH	CTLfut
NA	13.9[all]	9.8[all]	19.6[all]	15.5[all]
NEP	23.3[b,d]	14.3[a,c]	21.7[b,d]	15.1[a,c]
NI	5.7[d]	5.4[d]	6.9	8.3 [a,b]
NWP	19.3[b,c]	22.1[a,c]	14.5[all]	19.8 [c]
SA	1.1 [c,d]	1.5 [d]	2.3 [a]	2.4 [a,b]
SEP	1.8	2.5	1.9	2.0
SI	13.4[all]	10.2[all]	5.3[a,b]	5.5[a,b]
SWP	11.6[c]	13.1[c]	7.4[all]	11.4[c]

Appendix 2: Dependence of TC development on convective parametrization in climate models

While CLUBB, used in E3SM, has better performance in reproducing observed temperature and precipitation than the median across CMIP5 models, some biases remain, such as excessive tropical water vapor and underestimation of ice clouds in the midlatitudes (Guo et al. 2015). Qian et al. (2023) have investigated the sensitivity of E3SM version 1 to changes in 18 tunable parameters of cloud and convective parametrizations. They found that the relative importance of each parameter has a strong spatial dependence, with model improvements in one area often leading to degradation in other areas with different latitude, surface type, and/or cloud regime. There is evidence that differences in convection

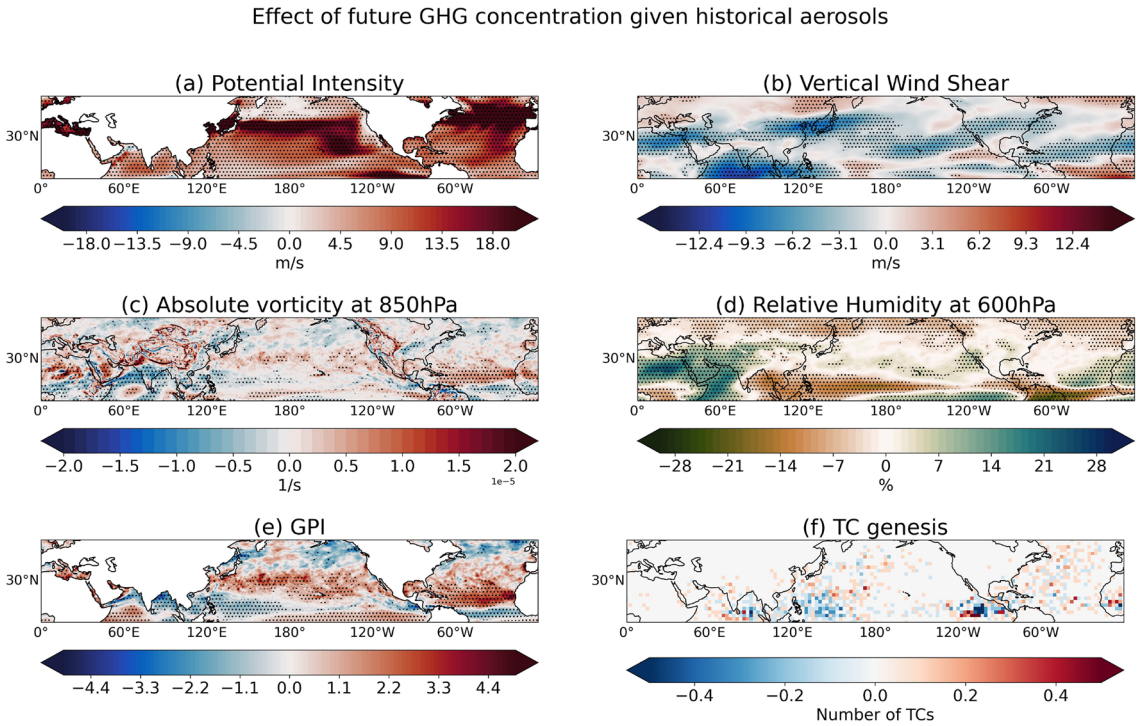

Fig. 11 Difference between the ASO-averaged, ensemble-mean of the ghgFaerH minus CTLhist experiments (representative of the effect of the change in GhGs given historical aerosols) for **a** potential intensity (m/s); **b** vertical wind shear between 850 and 200 hPa (m/s); **c** absolute vorticity at 850 hPa (s^{-1}), **d** relative humidity at 600 hPa (%), **e** GPI (dimensionless), and **f** TC genesis in a 2.5° grid (number of TCs). Stippling indicates significant anomalies at or above the 95% significance level for panels (**a**–**e**). Values are shown for the Northern Hemisphere

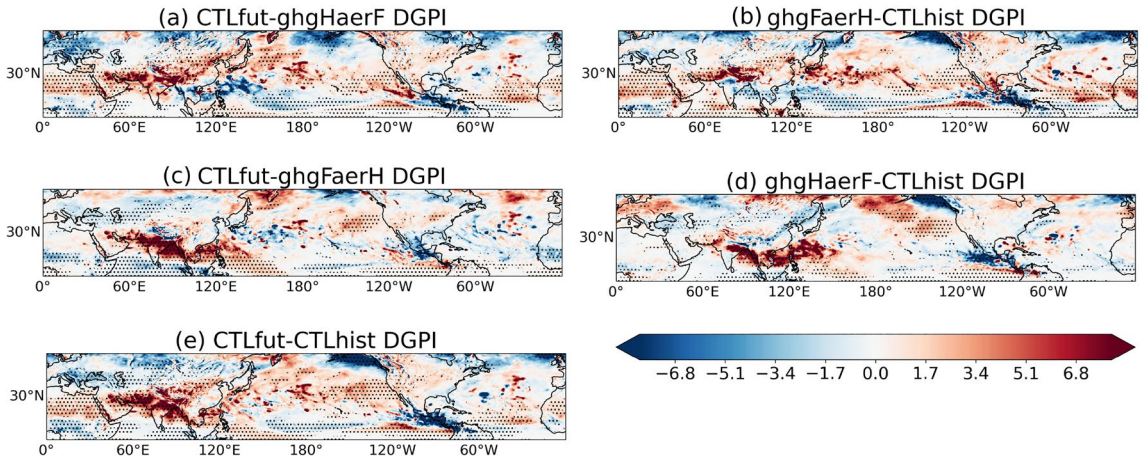

Fig. 12 Difference between the ASO-averaged, ensemble-mean DGPI (dimensionless) for **a** CTLfut minus ghgHaerF; **b** ghgFaerH minus CTLhist; **c** CTLfut minus ghgFaerH; **d** ghgHaerF minus CTLhist; and **e** CTLfut minus CTLhist. Panels **a**, **b** represent the responses due to changes in GhG, while panels **c**, **d** represent the changes due to the atmospheric effect of aerosols. Panel **e** represents the changes due to both future GhGs and aerosols. Stippling indicates significant anomalies at or above the 95% significance level

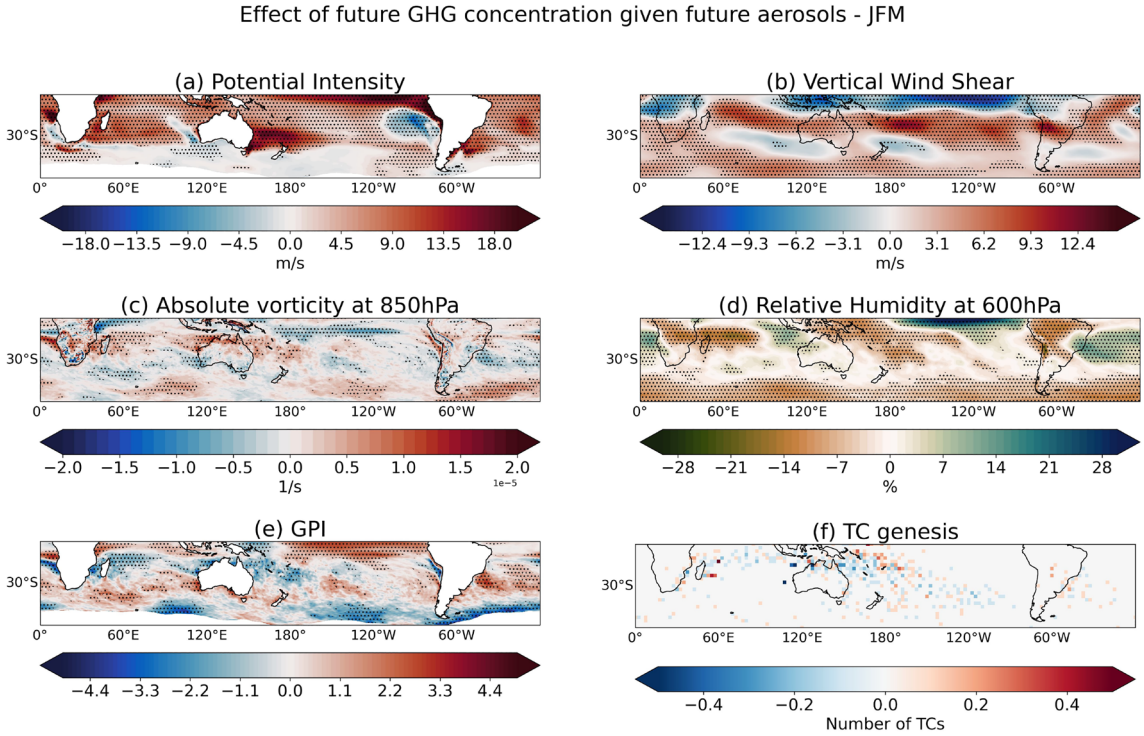

Fig. 13 Difference between the JFM-averaged, ensemble-mean of the CTLfut minus ghgHaerF experiments (representative of the effect of the change in GhGs given future aerosol) for **a** potential intensity (m/s); **b** vertical wind shear between 850 and 200 hPa (m/s); **c** absolute vorticity at 850 hPa (s^{-1}), **d** relative humidity at 600 hPa (%), **e** GPI, and **f** TC genesis in a 2.5° grid (number of TCs). Stippling indicates significant anomalies at or above the 95% significance level for panels (**a**–**e**). Values are shown for the Southern Hemisphere

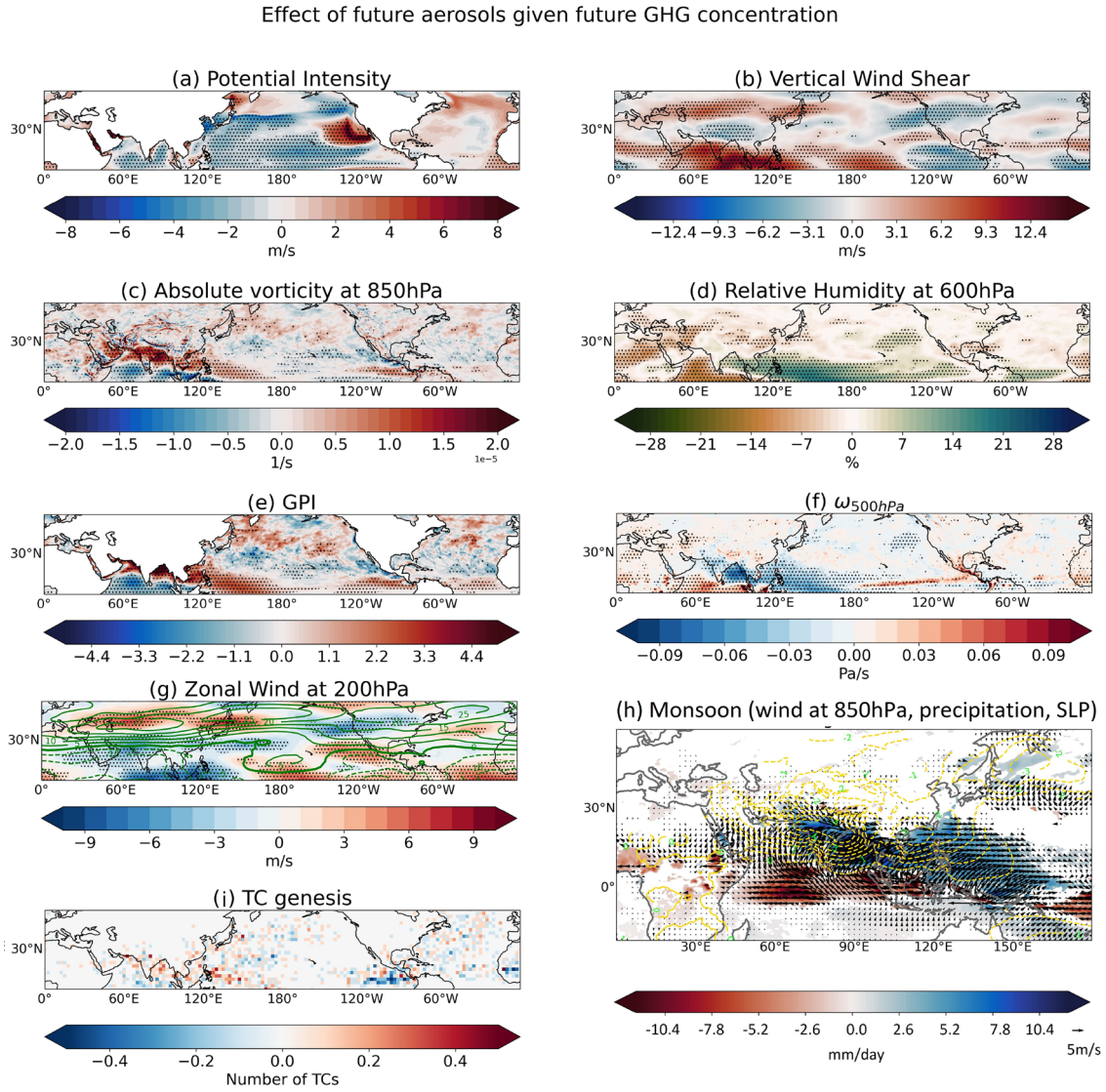

Fig. 14 Difference between the ASO-averaged, ensemble-mean of the CTLfut minus ghgFaerH experiments (representative of the atmospheric effects of future aerosol given future GhG) for for **a** potential intensity (m/s); **b** vertical wind shear between 850 hPa and 200 hPa (m/s); **c** absolute vorticity at 850 hPa (s^{-1}) and **d** relative humidity at 600 hPa (%); **e** Genesis potential index (GPI, dimensionless); **f** Pressure vertical velocity (omega) at 500 hPa (Pa/s); **g** zonal wind at 200 hPa (m/s). Contours in this panel shows the ensemble mean zonal wind at 200 hPa in the CTLhist experiment; **h** Sea level pressure (contour), precipitation (colors) and 850- hPa wind; **i** TC genesis in a 2.5° grid (number of TCs). For panels **a**–**g**, stippling indicates significant anomalies at or above the 95% significance level. In panel (**h**), the values are only shown for the North Indian and Northwestern Pacific, to focus on the monsoon, and only significant values are shown

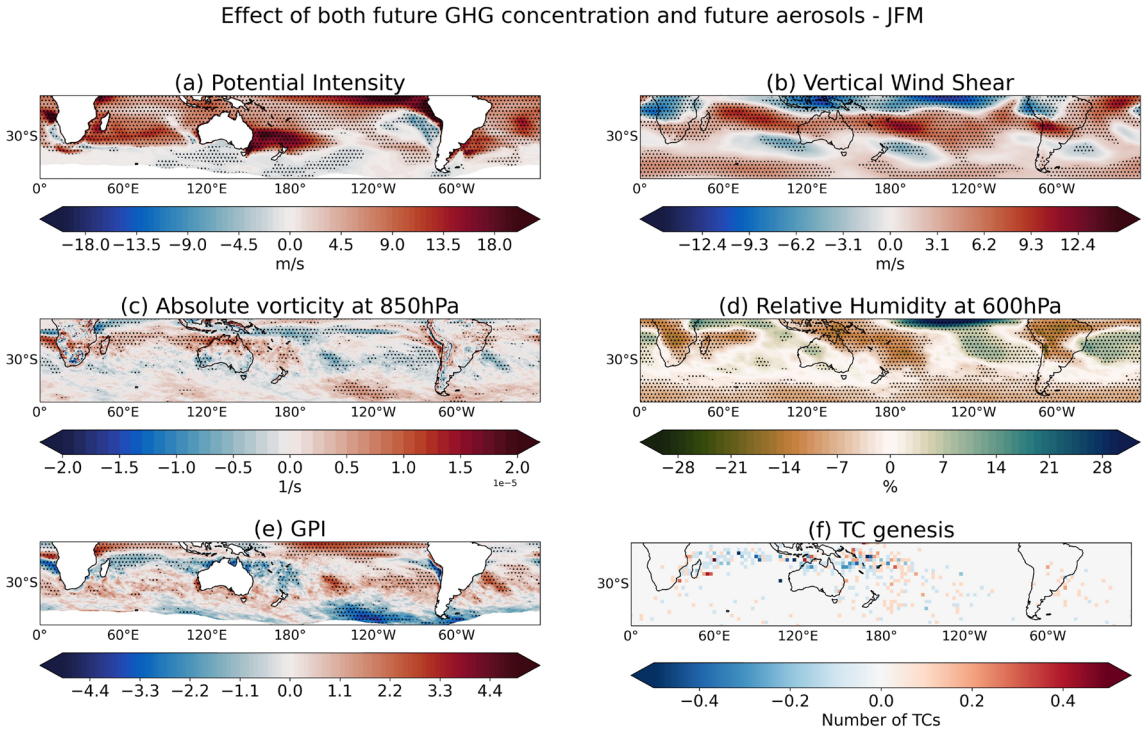

Fig. 15 Difference between the JFM-averaged, ensemble-mean of the CTLfut minus CTLhist experiments (representative of the effect of the changes in both GhGs and future aerosols) for **a** potential intensity (m/s); **b** vertical wind shear between 850 hPa and 200 hPa (m/s); **c** absolute vorticity at 850 hPa (s^{-1}), **d** relative humidity at 600 hPa (%), **e** GPI, and **f** TC genesis in a 2.5° grid (number of TCs). Stippling indicates significant anomalies at or above the 95% significance level for panels (**a**–**e**)

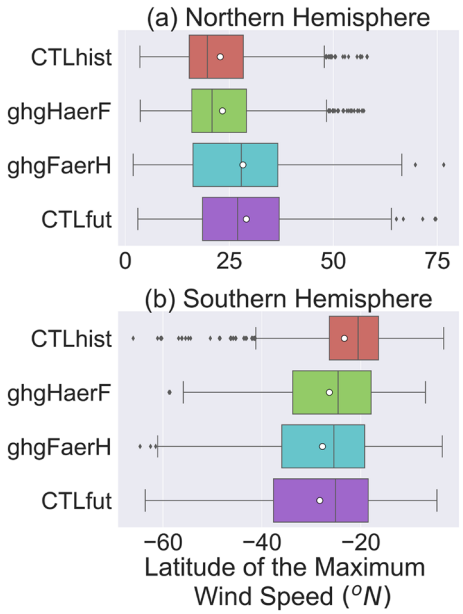

Fig. 16 Latitude of the maximum wind speed from the 10-member ensemble of each E3SM experiment in the Northern Hemisphere (left) and in the Southern Hemisphere (right). The edges of the boxplots show the 25th and 75th percentiles of the latitude of the maximum wind speed in the TCs. Whiskers represent 1.5 the interquartile range. Outliers are marked with diamond-shaped symbols. The median is marked as a straight line, and the mean is noted by a white circle. For both hemispheres, there are significant poleward displacement of the latitude of maximum wind speed with changes in GhG/SST (differences between CTLfut minus ghgHaerF, ghgFaerH minus CTLhist and CTLfut minus CTLhist), but not with future aerosols (CTLfut minus ghgFaerH and ghgHaerF minus CTLhist)

Table 8 Area-average ensemble mean percent change in precipitation for the experiments

	Precipitation (%)	Error
CTLfut-CTLhist	13.25	0.62
CTLfut-ghgHaerF	8.2	0.67
ghgFaerH-CTLhist	8.11	0.55
CTLfut-ghgFaerH	4.75	0.77
ghgHaerF-CTLhist	4.67	0.38

The values are shown over the ocean for the globe, averaged on the whole simultation year. The error correspond to deviations from the ensemble mean under the 95% confidence interval, and represent the variability between ensembles. Only regions equatorwise from 60° latitude were considered

schemes can also generate significant differences in TC frequency and intensity, though studies diverge on which parametrization parameters are more suitable to reproduce the TC frequency, depending on the model, parameters and area analyzed (Vitart and Stockdale 2001; Zhang and Wang 2018; Villafuerte et al. 2021; Fuentes-Franco et al. 2017; Russotto et al. 2022). There are a few possible explanations for these differences. Vitart and Stockdale (2001) suggested that uncertainties in global TC frequency due to convective parametrization, though generally small, are associated with the background stability of the atmosphere, with convective parametrizations with stronger/weaker background Convective Available Potential Energy (CAPE) producing more/less TCs. Zhao et al. (2012) suggested that the TC frequency in a high resolution global climate model is sensitive to the horizontal cumulus mixing rate parameter, through changes in the midtropospheric total convective mass flux and entrainment into the convective cores. An increase in cumulus mixing rate leads to a sharp increase in TC frequency initially, but to a decrease in TC frequency when the parameter gets to large values. They also suggested that TC frequency is sensitive to the strength of the damping of the horizontal flow, with increases in this parameter leading to more TCs being formed. Zhang and Wang (2018) suggested that the sensitivity of TC frequency and intensity in the North Pacific to convective parametrization schemes is explained by differences in the simulated low-level circulation. Simulations with convective parametrizations that produced more TCs had stronger low-level circulation between dry and wet columns, which was aided by stronger evaporative cooling associated with low-level clouds. Russotto et al. (2022) suggested that TC activity is sensitive to changes in the multipliers for the entrainment rates for the strongly entraining plumes in the cumulus convective parametrization, with increases in this parameter leading to more frequent and intense TCs. Fuentes-Franco et al. (2017) analyzed how TCs are represented with two different convection schemes over the CORDEX Central America domain and found that there are significant differences in TC density, duration, and intensity depending on convective parametrization, and that TCs are generally better represented in the North Atlantic than in the Northeast Pacific. Villafuerte et al. (2021) suggested that convective parametrizations with weaker, less frequent TCs over the Philippines have drier mid-tropospheric environments and smaller areas of positive low-level vorticity over the Pacific Ocean.

Table 9 Percent change in total TC precipitation due to future GhGs, globally for all TCs, calculated as the radially-averaged TCP at 25 km, at 50 km, 100 km, 400 km and 500 km from the center of the TC

	Atmospheric effect of future aerosols given			
	Historical GhGs		Future GhGs	
	Precipitation (%)	Error (%)	Precipitation (%)	Error (%)
TCP25 km	− 12.2	6.0	− 8.3	6.4
TCP50 km	− 6.6	5.8	− 1.9	6.1
TCP100 km	9.9	5.2	15.7	5.4
TCP400 km	14.9	5.0	19.5	5.2
TCP500 km	9.8	5.0	14.1	5.6
	Effect of future GhGs given			
	Historical aerosols		Future aerosols	
	Precipitation (%)	Error (%)	Precipitation (%)	Error (%)
TCP25 km	11.5	1.8	13.3	2.1
TCP50 km	9.9	1.6	11.7	2.0
TCP100 km	7.8	1.5	9.5	1.8
TCP400 km	5.4	1.4	6.7	1.5
TCP500 km	5.3	1.4	6.5	1.5

The response due to the atmospheric effect of future aerosols is shown on the top, given historical GhGs (difference between the ghgHaerF minus the CTLhist) and given future GhGs (CTLfut and ghgFaerH). The response due to future GhGs is shown on the bottom, given historical aerosols (difference between the ghgFaerH minus the CTLhist) and given future aerosols (CTLfut and ghgHaerF). The margin of error corresponds to deviation from the mean under the 95% confidence interval

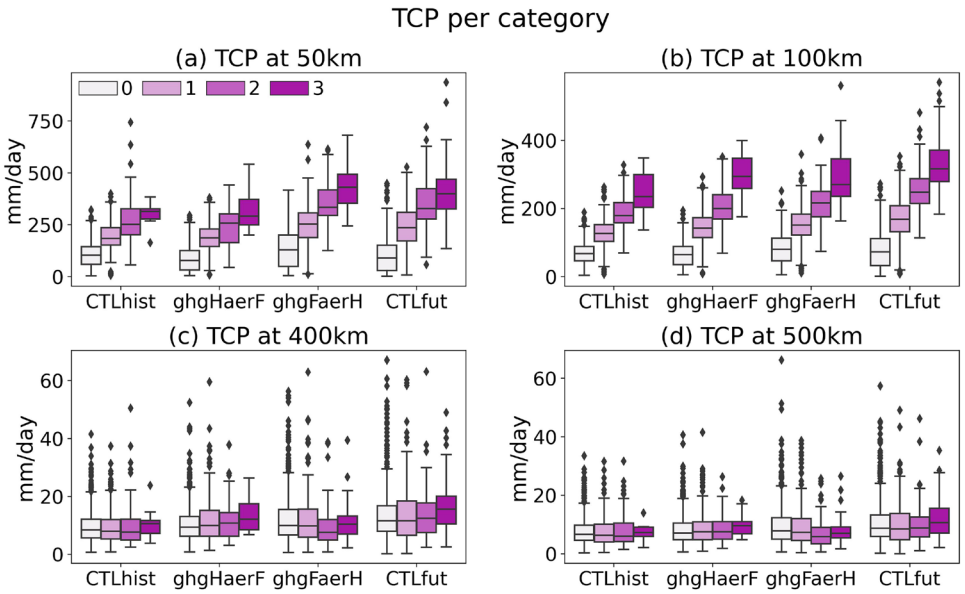

Fig. 17 Boxplot of the mean TCP in each experiment, divided by categories according to the Saffir–Simpson scale radially averaged TCP at: **a** 50 km, **b** 100 km, **c** 400 km, **d** 500 km from the center of the TC. The boxplot represents the internal variability of the experiments for all TCs in the 10 ensemble members in each experiment. The edges of the boxplots show the 25th and 75th percentiles. Whiskers represent 1.5 the interquartile range. Outliers are marked with diamond-shaped symbols. The median is marked as a straight line

Table 10 Area-average ensemble mean difference in mean precipitation in each basin (in mm/day and percent), total TCP ($r < 500$ km, in percentage) and TC frequency (in TCs/year) for the atmosphere effect of aerosols given historical GhGs (ghgHaerF minus CTLhist) and future GhGs (CTLfut minus ghgFaerH)

Atmospheric effects of future aerosols								
	Historical GhGs				Future GhGs			
	Precipitation		TCP	TCF	Precipitation		TCP	TCF
	(mm/day)	(%)	(%)	(TCs/y)	(mm/day)	(%)	(%)	(TCs/y)
NA	0.07	1.9	− 2.2	− 4.4*	− 0.07	− 1.6	− 1.0	− 6.0*
NEP	− 0.06	− 1.5	2.7	− 10.4*	0.06	1.5	4.7	− 8.7*
NWP	1.23	27.7*	44.1*	4.8*	1.60	35.1*	53.3*	8.5*
NI	0.34	13.8*	7.1	0.3	0.81	21.2*	25.1*	1.7
SI	0.24	7.8*	6	− 3.2*	0.28	8.6*	11.0	1.5
SWP	0.24	6.5	− 3.5	− 0.8	0.26	6.5*	13.8*	3

The changes in background precipitation are shown for the most common TC season in each hemisphere (ASO for the northern hemisphere and JFM for the southern hemisphere). Only regions over the ocean and equatorwise from 60° latitude were considered. Significant values at or above the 95% confidence level are marked with an asterisk

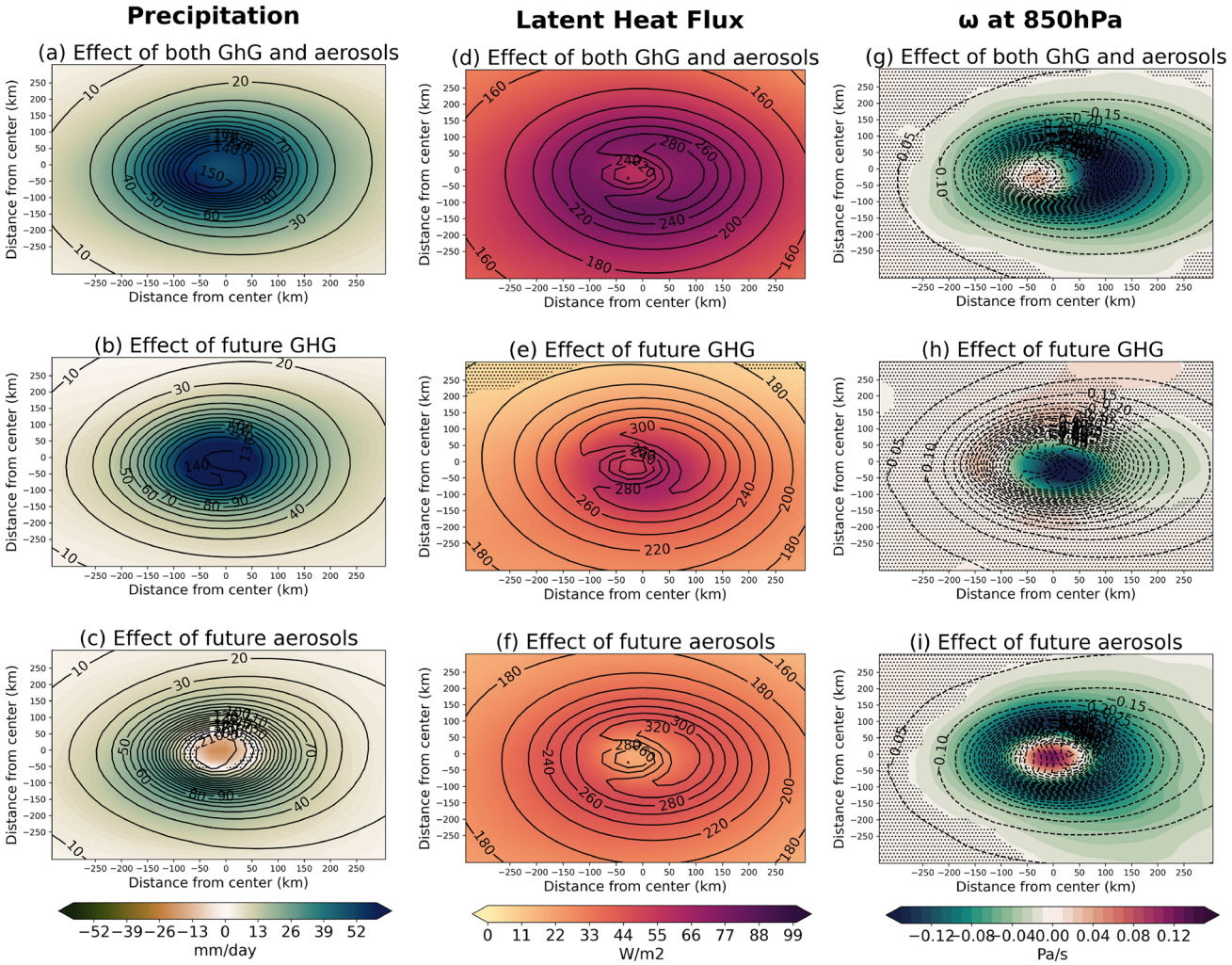

Fig. 18 Difference between the mean precipitation within a 300 km radius of the TCs for **a** CTLfut minus CTLhist experiments, representative of the effect of changing both aerosols and GhG/SST (colors), and mean values in the CTLhist experiment (contours); **b** CTLfut minus ghgHaerF experiments (colors), representative of the effect of future GhGs given future aerosols, and mean values in the ghgHaerF experiment (contours); **c** ghg2100aer2100 minus CTLhist, representative of the atmospheric effect of the future aerosols given historical GhGs (colors), and mean values in the CTLhist experiment (contours); **d–f** Same as **a–c**, but for Surface Latent Heat Flux (W/m^2); **g–i** Same as **a–c**, but for vertical velocity in pressure coordinates (Pa/s) at 850 hPa. Stippling represents areas where the differences are not significant at the 95% confidence level

Acknowledgements This material is based upon work supported by the U.S. Department of Energy (DOE), Office of Science, Office of Biological and Environmental Research (BER), Earth and Environmental Systems Modeling (EESM) Program, under Early Career Research Program Award Number DE-SC0021109. This research used resources of the National Energy Research Scientific Computing Center (NERSC), a U.S. Department of Energy Office of Science User Facility located at Lawrence Berkeley National Laboratory, operated under Contract No. DE-AC02-05CH11231. E3SM simulations were performed using BER Earth System Modeling program's Compy computing cluster located at Pacific Northwest National Laboratory. PNNL is operated by Battelle for the U.S. Department of Energy under Contract DE-AC05-76RL01830. E3SM data and model were obtained from the Energy Exascale Earth System Model project, sponsored by the U.S.Department of Energy, Office of Science, Office of Biological and Environmental Research. We thank DOE's RGMA program area, the Data Management program, and NERSC for making this coordinated CMIP6 analysis activity possible. We acknowledge the World Climate Research Programme, which, through its Working Group on Coupled Modelling, coordinated and promoted CMIP6. We thank the climate modeling groups for producing and making available their model output, the Earth System Grid Federation (ESGF) for archiving the data and providing access, and the multiple funding agencies who support CMIP6 and ESGF. AHS and SJC acknowledge support from DOE Grant DE-SC0023333. SJC also acknowledges support of National Science Foundation (NSF) Grants AGS 20-43142 and 22-44918, as well National Oceanic and Atmospheric Administration (NOAA) Grants NA21OAR4310345 and NA22OAR4310610. We thank three anonymous reviewers for their constructive comments which have helped improve the manuscript.

Author contributions Sena ran the simulations, performed analysis, interpreted results, and wrote the manuscript. Patricola obtained funding, conceived the study, interpreted results and contributed to the manuscript. Camargo interpreted results, and contributed to the manuscript. Sobel interpreted results, and contributed to the manuscript. All authors commented on previous versions of the manuscript. All authors approved the final manuscript.

Funding This material is based upon work supported by the U.S. Department of Energy (DOE), Office of Science, Office of Biological and Environmental Research (BER), Earth and Environmental Systems Modeling (EESM) Program, under Early Career Research Program Award Number DE-SC0021109. This research used resources of the National Energy Research Scientific Computing Center (NERSC), a U.S. Department of Energy Office of Science User Facility located at Lawrence Berkeley National Laboratory, operated under Contract No. DE-AC02-05CH11231. E3SM simulations were performed using BER Earth System Modeling program's Compy computing cluster located at Pacific Northwest National Laboratory. PNNL is operated by Battelle for the U.S. Department of Energy under Contract DE-AC05-76RL01830. AHS and SJC acknowledge support from DOE Grant DE-SC0023333. SJC also acknowledges support of National Science Foundation (NSF) Grants AGS 20-43142 and 22-44918, as well National Oceanic and Atmospheric Administration (NOAA) Grants NA21OAR4310345 and NA22OAR4310610.

Data availability HadISST data can be accessed at https://www.metoffice.gov.uk/hadobs/hadisst/. E3SM version 2 is available at https://e3sm.org (DOI: https://doi.org/10.11578/E3SM/dc.20210927.1). TECA is available at https://teca.readthedocs.io/en/latest/index.html (DOI: https://doi.org/10.5281/zenodo.6640287). The model output used in this manuscript is published at https://doi.org/10.5281/zenodo.10835535 (DOI: https://doi.org/10.5281/zenodo.10835535).

Declarations

Conflict interest The authors have no relevant financial or non-financial interests to disclose.

References

Balaguru K, Leung LR, Roekel LPV, Golaz J-C, Ullrich PA, Caldwell PM, Hagos SM, Harrop BE, Mametjanov A (2020) Characterizing tropical cyclones in the energy Exascale earth system model version 1. J Adv Model Earth Syst 12(8):2019–002024. https://doi.org/10.1029/2019MS002024

Balaguru K, Foltz GR, Leung LR, Hagos SM (2022) Impact of rainfall on tropical cyclone-induced sea surface cooling. Geophys Res Lett 49(10):2022–098187. https://doi.org/10.1029/2022GL098187

Bender MA, Ginis I (2000) Real-case simulations of hurricane-ocean interaction using a high-resolution coupled model: effects on hurricane intensity. Monthly Weather Rev 128(4):917–946. https://doi.org/10.1175/1520-0493(2000)128<0917:RCSOHO>2.0.CO;2. Publisher: American Meteorological Society Section: Monthly Weather Review. Accessed 2022-06-14

Bloemendaal N, Moel Hd, Mol JM, Bosma PRM, Polen AN, Collins JM (2021) Adequately reflecting the severity of tropical cyclones using the new Tropical Cyclone Severity Scale. Environ Res Lett 16(1):014048. https://doi.org/10.1088/1748-9326/abd131. Publisher: IOP Publishing. Accessed 2022-09-27

Bony S, Bellon G, Klocke D, Sherwood S, Fermepin S, Denvil S (2013) Robust direct effect of carbon dioxide on tropical circulation and regional precipitation. Nat Geosci 6(6):447–451. https://doi.org/10.1038/ngeo1799. Number: 6 Publisher: Nature Publishing Group. Accessed 2023-11-20

Booth BBB, Dunstone NJ, Halloran PR, Andrews T, Bellouin N (2012) Aerosols implicated as a prime driver of twentieth-century North Atlantic climate variability. Nature 484(7393):228–232. https://doi.org/10.1038/nature10946

Calvin K, Bond-Lamberty B, Clarke L, Edmonds J, Eom J, Hartin C, Kim S, Kyle P, Link R, Moss R, McJeon H, Patel P, Smith S, Waldhoff S, Wise M (2017) The SSP4: a world of deepening inequality. Global Environ Change 42:284–296. https://doi.org/10.1016/j.gloenvcha.2016.06.010. Accessed 2024-01-18

Caldwell PM, Mametjanov A, Tang Q, Roekel LPV, Golaz J-C, Lin W, Bader DC, Keen ND, Feng Y, Jacob R, Maltrud ME, Roberts AF, Taylor MA, Veneziani M, Wang H, Wolfe JD, Balaguru K, Cameron-Smith P, Dong L, Klein SA, Leung LR, Li H-Y, Li Q, Liu X, Neale RB, Pinheiro M, Qian Y, Ullrich PA, Xie S, Yang Y, Zhang Y, Zhang K, Zhou T (2019a) The DOE E3SM coupled model version 1: description and results at high resolution. J

Adv Model Earth Syst 11(12):4095–4146. https://doi.org/10.1029/2019MS001870. Accessed 2021-07-27

Caldwell PM, Mametjanov A, Tang Q, Van Roekel LP, Golaz J-C, Lin W, Bader DC, Keen ND, Feng Y, Jacob R, Maltrud ME, Roberts AF, Taylor MA, Veneziani M, Wang H, Wolfe JD, Balaguru K, Cameron-Smith P, Dong L, Klein SA, Leung LR, Li H-Y, Li Q, Liu X, Neale RB, Pinheiro M, Qian Y, Ullrich PA, Xie S, Yang Y, Zhang Y, Zhang K, Zhou T (2019b) The DOE E3SM coupled model version 1: description and results at high resolution. J Adv Model Earth Syst 11(12):4095–4146. https://doi.org/10.1029/2019MS001870. _eprint: https://onlinelibrary.wiley.com/doi/pdf/10.1029/2019MS001870. Accessed 2023-10-18

Camargo SJ (2013) Global and regional aspects of tropical cyclone activity in the CMIP5 models. J Climate 26(24):9880–9902. https://doi.org/10.1175/JCLI-D-12-00549.1. Publisher: American Meteorological Society Section: Journal of Climate. Accessed 2022-08-29

Camargo SJ, Emanuel KA, Sobel AH (2007) Use of a genesis potential index to diagnose ENSO effects on tropical cyclone genesis. J Climate 20(19):4819–4834. https://doi.org/10.1175/JCLI4282.1. Publisher: American Meteorological Society Section: Journal of Climate

Camargo SJ, Tippett MK, Sobel AH, Vecchi GA, Zhao M (2014) Testing the performance of tropical cyclone genesis indices in future climates using the HiRAM model. J Climate 27(24):9171–9196. https://doi.org/10.1175/JCLI-D-13-00505.1. Publisher: American Meteorological Society Section: Journal of Climate. Accessed 2024-01-18

Camargo SJ, Murakami H, Bloemendaal N, Chand SS, Deshpande MS, Dominguez-Sarmiento C, González-Alemán JJ, Knutson TR, Lin I-I, Moon I-J, Patricola CM, Reed KA, Roberts MJ, Scoccimarro E, Tam CYF, Wallace EJ, Wu L, Yamada Y, Zhang W, Zhao H (2023) An update on the influence of natural climate variability and anthropogenic climate change on tropical cyclones. Trop Cyclone Res Rev 12(3):216–239. https://doi.org/10.1016/j.tcrr.2023.10.001. Accessed 2024-01-18

Cao J, Zhao H, Wang B, Wu L (2021) Hemisphere-asymmetric tropical cyclones response to anthropogenic aerosol forcing. Nat Commun 12(1):6787. https://doi.org/10.1038/s41467-021-27030-z. Number: 1 Publisher: Nature Publishing Group. Accessed 2023-01-20

Chadwick R, Good P, Andrews T, Martin G (2014) Surface warming patterns drive tropical rainfall pattern responses to CO2 forcing on all timescales. Geophys Res Lett 41(2):610–615. https://doi.org/10.1002/2013GL058504. _eprint: https://onlinelibrary.wiley.com/doi/pdf/10.1002/2013GL058504. Accessed 2023-12-14

Chan JCL, Liu KS (2022) Recent decrease in the difference in tropical cyclone occurrence between the Atlantic and the Western North Pacific. Adv Atmos Sci 39(9):1387–1397. https://doi.org/10.1007/s00376-022-1309-x. Accessed 2024-03-08

Chand SS, Walsh KJE, Camargo SJ, Kossin JP, Tory KJ, Wehner MF, Chan JCL, Klotzbach PJ, Dowdy AJ, Bell SS, Ramsay HA, Murakami H (2022) Declining tropical cyclone frequency under global warming. Nat Climate Change, 1–7. https://doi.org/10.1038/s41558-022-01388-4. Publisher: Nature Publishing Group. Accessed 2022-06-27

Chen Z, Zhou T, Zhang L, Chen X, Zhang W, Jiang J (2020) Global land monsoon precipitation changes in CMIP6 projections. Geophys Res Lett 47(14):2019–086902. https://doi.org/10.1029/2019GL086902. _eprint: https://onlinelibrary.wiley.com/doi/pdf/10.1029/2019GL086902. Accessed 2024-03-08

Daloz AS, Camargo SJ (2018) Is the poleward migration of tropical cyclone maximum intensity associated with a poleward migration of tropical cyclone genesis? Climate Dyn 50(1):705–715. https://doi.org/10.1007/s00382-017-3636-7. Accessed 2023-06-05

Davis CA (2018) Resolving tropical cyclone intensity in models. Geophys Res Lett 45(4):2082–2087. https://doi.org/10.1002/2017GL076966. _eprint: https://onlinelibrary.wiley.com/doi/pdf/10.1002/2017GL076966. Accessed 2023-06-12

Dunstone NJ, Smith DM, Booth BBB, Hermanson L, Eade R (2013) Anthropogenic aerosol forcing of Atlantic tropical storms. Nat Geosci 6(7):534–539. https://doi.org/10.1038/ngeo1854. Publisher: Nature Publishing Group. Accessed 2024-03-19

Ekman AML (2014) Do sophisticated parameterizations of aerosol-cloud interactions in CMIP5 models improve the representation of recent observed temperature trends? J Geophys Res Atmos 119(2):817–832. https://doi.org/10.1002/2013JD020511. _eprint: https://onlinelibrary.wiley.com/doi/pdf/10.1002/2013JD020511. Accessed 2023-11-28

Emanuel KA (1988) The maximum intensity of hurricanes. J Atmos Sci 45(7):1143–1155

Emanuel K (2005) Increasing destructiveness of tropical cyclones over the past 30 years. Nature 436(7051):686–688. https://doi.org/10.1038/nature03906. Number: 7051 Publisher: Nature Publishing Group. Accessed 2022-04-04

Emanuel K, Nolan DS (2004) Tropical cyclone activity and the global climate system: 26th Conference on Hurricanes and Tropical Meteorolgy, pp. 240–241. http://www.scopus.com/inward/record.url?scp=3042740008 &partnerID=8YFLogxK. Accessed 2022-03-15

Emanuel KA, Sobel AH (2013) Response of tropical sea surface temperature, precipitation, and tropical cyclone-related variables to changes in global and local forcing. J Adv Model Earth Syst 5:447–458

Eyring V, Bony S, Meehl GA, Senior CA, Stevens B, Stouffer RJ, Taylor KE (2016) Overview of the coupled model intercomparison project phase 6 (CMIP6) experimental design and organization. Geosci Model Develop 9(5):1937–1958. https://doi.org/10.5194/gmd-9-1937-2016. Accessed 2021-08-18

Fan J, Wang Y, Rosenfeld D, Liu X (2016) Review of aerosol-cloud interactions: mechanisms, significance, and challenges. J Atmos Sci 73(11):4221–4252. https://doi.org/10.1175/JAS-D-16-0037.1. Publisher: American Meteorological Society Section: Journal of the Atmospheric Sciences. Accessed 2023-11-28

Fiedler S, Stevens B, Gidden M, Smith SJ, Riahi K, Vuuren D (2019) First forcing estimates from the future CMIP6 scenarios of anthropogenic aerosol optical properties and an associated Twomey effect. Geosci Model Develop 12(3):989–1007. https://doi.org/10.5194/gmd-12-989-2019. Publisher: Copernicus GmbH. Accessed 2023-11-29

Fiedler S, Noije T, Smith CJ, Boucher O, Dufresne J-L, Kirkevåg A, Olivié D, Pinto R, Reerink T, Sima A, Schulz M (2023) Historical changes and reasons for model differences in anthropogenic aerosol forcing in CMIP6. Geophys Res Lett 50(15):2023–104848. https://doi.org/10.1029/2023GL104848. _eprint: https://onlinelibrary.wiley.com/doi/pdf/10.1029/2023GL104848. Accessed 2023-11-29

Fuentes-Franco R, Giorgi F, Coppola E, Zimmermann K (2017) Sensitivity of tropical cyclones to resolution, convection scheme and ocean flux parameterization over Eastern Tropical Pacific and Tropical North Atlantic Oceans in the RegCM4 model. Climate Dyn 49(1):547–561. https://doi.org/10.1007/s00382-016-3357-3. Accessed 2023-11-20

Giorgi F, Raffaele F, Coppola E (2019) The response of precipitation characteristics to global warming from climate projections. Earth Syst Dyna 10(1):73–89. https://doi.org/10.5194/esd-10-73-2019. Accessed 2023-10-02

Fujimori S, Hasegawa T, Masui T, Takahashi K, Herran DS, Dai H, Hijioka Y, Kainuma M (2017) SSP3: AIM implementation of Shared Socioeconomic Pathways. Global Environ Change

42:268–283. https://doi.org/10.1016/j.gloenvcha.2016.06.009. Accessed 2024-01-18

Golaz J-C, Larson VE, Cotton WR (2002) A PDF-based model for boundary layer clouds. Part I: method and model description. J Atmos Sci 59(24):3540–3551. https://doi.org/10.1175/1520-0469(2002)059<3540:APBMFB>2.0.CO;2. Publisher: American Meteorological Society Section: Journal of the Atmospheric Sciences. Accessed 2023-10-12

Golaz J-C, Caldwell PM, Roekel LPV, Petersen MR, Tang Q, Wolfe JD, Abeshu G, Anantharaj V, Asay-Davis XS, Bader DC, Baldwin SA, Bisht G, Bogenschutz PA, Branstetter M, Brunke MA, Brus SR, Burrows SM, Cameron-Smith PJ, Donahue AS, Deakin M, Easter RC, Evans KJ, Feng Y, Flanner M, Foucar JG, Fyke JG, Griffin BM, Hannay C, Harrop BE, Hoffman MJ, Hunke EC, Jacob RL, Jacobsen DW, Jeffery N, Jones PW, Keen ND, Klein SA, Larson VE, Leung LR, Li H-Y, Lin W, Lipscomb WH, Ma P-L, Mahajan S, Maltrud ME, Mametjanov A, McClean JL, McCoy RB, Neale RB, Price SF, Qian Y, Rasch PJ, Eyre JEJR, Riley WJ, Ringler TD, Roberts AF, Roesler EL, Salinger AG, Shaheen Z, Shi X, Singh B, Tang J, Taylor MA, Thornton PE, Turner AK, Veneziani M, Wan H, Wang H, Wang S, Williams DN, Wolfram PJ, Worley PH, Xie S, Yang Y, Yoon J-H, Zelinka MD, Zender CS, Zeng X, Zhang C, Zhang K, Zhang Y, Zheng X, Zhou T, Zhu Q (2019) The DOE E3SM coupled model version 1: overview and evaluation at standard resolution. J Adv Model Earth Syst 11(7):2089–2129. https://doi.org/10.1029/2018MS001603. Accessed 2021-07-21

Golaz J-C, Van Roekel LP, Zheng X, Roberts AF, Wolfe JD, Lin W, Bradley AM, Tang Q, Maltrud ME, Forsyth RM, Zhang C, Zhou T, Zhang K, Zender CS, Wu M, Wang H, Turner AK, Singh B, Richter JH, Qin Y, Petersen MR, Mametjanov A, Ma P-L, Larson VE, Krishna J, Keen ND, Jeffery N, Hunke EC, Hannah WM, Guba O, Griffin BM, Feng Y, Engwirda D, Di Vittorio AV, Dang C, Conlon LM, Chen C-C-J, Brunke MA, Bisht G, Benedict JJ, Asay-Davis XS, Zhang Y, Zhang M, Zeng X, Xie S, Wolfram PJ, Vo T, Veneziani M, Tesfa TK, Sreepathi S, Salinger AG, Reeves Eyre JEJ, Prather MJ, Mahajan S, Li Q, Jones PW, Jacob RL, Huebler GW, Huang X, Hillman BR, Harrop BE, Foucar JG, Fang Y, Comeau DS, Caldwell PM, Bartoletti T, Balaguru K, Taylor MA, McCoy RB, Leung LR, Bader DC (2022) The DOE E3SM model version 2: overview of the physical model and initial model evaluation. J Adv Model Earth Syst 14(12), 2022–003156 https://doi.org/10.1029/2022MS003156. _eprint: https://onlinelibrary.wiley.com/doi/pdf/10.1029/2022MS003156. Accessed 2023-10-12

Goldenberg SB, Landsea CW, Mestas-Nuñez AM, Gray WM (2001) The recent increase in Atlantic hurricane activity: causes and implications. Science 293(5529):474–479

Guo H, Golaz J-C, Donner LJ, Wyman B, Zhao M, Ginoux P (2015a) CLUBB as a unified cloud parameterization: opportunities and challenges. Geophys Res Lett 42(11):4540–4547. https://doi.org/10.1002/2015GL063672. _eprint: https://onlinelibrary.wiley.com/doi/pdf/10.1002/2015GL063672. Accessed 2023-11-28

Guo L, Turner AG, Highwood EJ (2015b) Impacts of 20th century aerosol emissions on the South Asian monsoon in the CMIP5 models. Atmos Chem Phys 15(11):6367–6378. https://doi.org/10.5194/acp-15-6367-2015. Publisher: Copernicus GmbH. Accessed 2023-03-21

Guzman O, Jiang H (2021) Global increase in tropical cyclone rain rate. Nat Commun 12(1):5344. https://doi.org/10.1038/s41467-021-25685-2. Number: 1 Publisher: Nature Publishing Group. Accessed 2023-02-01

Hausfather Z, Peters GP (2020) Emissions—the 'business as usual' story is misleading. Nature 577(7792):618–620. https://doi.org/10.1038/d41586-020-00177-3. Bandiera_abtest: a Cg_type: Comment Number: 7792 Publisher: Nature Publishing Group Subject_term: Climate change, Climate sciences, Energy, Policy, Society. Accessed 2024-01-18

Hazra A, Mukhopadhyay P, Taraphdar S, Chen J-P, Cotton WR (2013) Impact of aerosols on tropical cyclones: an investigation using convection-permitting model simulation. J Geophys Res Atmos 118(13):7157–7168. https://doi.org/10.1002/jgrd.50546. _eprint: https://onlinelibrary.wiley.com/doi/pdf/10.1002/jgrd.50546. Accessed 2022-07-05

Held IM, Zhao M (2011) The response of tropical cyclone statistics to an increase in CO_2 with fixed sea surface temperatures. J Climate 24(20):5353–5364. https://doi.org/10.1175/JCLI-D-11-00050.1. Publisher: American Meteorological Society Section: Journal of Climate. Accessed 2023-11-20

Hsu W-C, Patricola CM, Chang P (2019) The impact of climate model sea surface temperature biases on tropical cyclone simulations. Climate Dyn 53(1):173–192. https://doi.org/10.1007/s00382-018-4577-5. Accessed 2022-04-04

IPCC (2021) Summary for policymakers. In: Masson-Delmotte V, Zhai P, Pirani A, Connors SL, Péan C, Berger S, Caud N, Chen Y, Goldfarb L, Gomis MI, Huang M, Leitzell K, Lonnoy E, Matthews JBR, Maycock TK, Waterfield T, Yelekçi K, Yu R, Zhu B (eds) Climate change 2021: the physical science basis. Contribution of working group I to the sixth assessment report of the intergovernmental panel on climate change. Cambridge University Press, Cambridge, United Kingdom and New York, NY, USA, pp 3–32. https://doi.org/10.1017/9781009157896.001. https://www.ipcc.ch/report/ar6/wg1/

Jin C, Wang B, Liu J (2020) Future changes and controlling factors of the eight regional monsoons projected by CMIP6 models. J Climate 33(21):9307–9326. https://doi.org/10.1175/JCLI-D-20-0236.1. Publisher: American Meteorological Society Section: Journal of Climate. Accessed 2024-03-11

Karnauskas KB, Zhang L, Emanuel KA (2021) The Feedback of cold wakes on tropical cyclones. Geophys Res Lett. https://doi.org/10.1029/2020GL091676. Accessed 2021-09-13

Khain AP, Beheng KD, Heymsfield A, Korolev A, Krichak SO, Levin Z, Pinsky M, Phillips V, Prabhakaran T, Teller A, Heever SC, Yano J-I (2015) Representation of microphysical processes in cloud-resolving models: Spectral (bin) microphysics versus bulk parameterization. Rev Geophys 53(2):247–322. https://doi.org/10.1002/2014RG000468. _eprint: https://onlinelibrary.wiley.com/doi/pdf/10.1002/2014RG000468. Accessed 2023-11-28

Khouakhi A, Villarini G, Vecchi GA (2017) Contribution of tropical cyclones to rainfall at the global scale. J. Climate 30(1):359–372. https://doi.org/10.1175/JCLI-D-16-0298.1. Publisher: American Meteorological Society Section: Journal of Climate. Accessed 2023-06-12

Klotzbach PJ, Wood KM, Bell MM, Blake ES, Bowen SG, Caron L-P, Collins JM, Gibney EJ, Schreck CJ, Truchelut RE (2022a) A hyperactive end to the Atlantic hurricane season October–November 2020. Bull Am Meteorol Soc 103(1):110–128. https://doi.org/10.1175/BAMS-D-20-0312.1. Accessed 2022-02-04

Klotzbach PJ, Wood KM, Schreck CJ III, Bowen SG, Patricola CM, Bell MM (2022b) Trends in global tropical cyclone activity: 1990–2021. Geophys Res Lett 49(6):2021–095774. https://doi.org/10.1029/2021GL095774. _eprint: https://onlinelibrary.wiley.com/doi/pdf/10.1029/2021GL095774. Accessed 2022-04-01

Knutson TR, Sirutis JJ, Vecchi GA, Garner S, Zhao M, Kim H-S, Bender M, Tuleya RE, Held IM, Villarini G (2013) Dynamical downscaling projections of twenty-first-century Atlantic hurricane activity: CMIP3 and CMIP5 model-based scenarios. J Climate 26(17):6591–6617. https://doi.org/10.1175/JCLI-D-12-00539.1. Publisher: American Meteorological Society Section: Journal of Climate. Accessed 2023-01-19

Knutson TR, Sirutis JJ, Zhao M, Tuleya RE, Bender M, Vecchi GA, Villarini G, Chavas D (2015) Global projections of intense

tropical cyclone activity for the late twenty-first century from dynamical downscaling of CMIP5/RCP4.5 scenarios. J Climate 28(18):7203–7224. https://doi.org/10.1175/JCLI-D-15-0129.1. Publisher: American Meteorological Society Section: Journal of Climate. Accessed 2023-01-19

Knutson T, Camargo SJ, Chan JCL, Emanuel K, Ho C-H, Kossin J, Mohapatra M, Satoh M, Sugi M, Walsh K, Wu L (2019) Tropical cyclones and climate change assessment: part I: detection and attribution. Bull Am Meteorol Soc 100(10):1987–2007. https://doi.org/10.1175/BAMS-D-18-0189.1. Accessed 2022-02-24

Knutson T, Camargo SJ, Chan JCL, Emanuel K, Ho C-H, Kossin J, Mohapatra M, Satoh M, Sugi M, Walsh K, Wu L (2020) Tropical cyclones and climate change assessment: part II: projected response to anthropogenic warming. Bull Am Meteorol Soc 101(3):303–322. https://doi.org/10.1175/BAMS-D-18-0194.1. Publisher: American Meteorological Society Section: Bulletin of the American Meteorological Society. Accessed 2021-07-23

Korty RL, Emanuel KA, Scott JR (2008) Tropical cyclone-induced upper-ocean mixing and climate: application to equable climates. J Climate 21(4):638–654. https://doi.org/10.1175/2007JCLI1659.1. Publisher: American Meteorological Society Section: Journal of Climate. Accessed 2024-05-14

Kossin JP, Emanuel KA, Vecchi GA (2014) The poleward migration of the location of tropical cyclone maximum intensity. Nature 509(7500):349–352. https://doi.org/10.1038/nature13278. Accessed 2021-07-29

Kossin JP, Knapp KR, Olander TL, Velden CS (2020) Global increase in major tropical cyclone exceedance probability over the past four decades. Proc Natl Acad Sci 117(22):11975–11980. https://doi.org/10.1073/pnas.1920849117. Publisher: Proceedings of the National Academy of Sciences. Accessed 2022-06-21

Krall GM, Cottom WR (2012) Potential indirect effects of aerosol on tropical cyclone intensity: convective fluxes and cold-pool activity. Atmos Chem Phys Discus 12(1):351–385. https://doi.org/10.5194/acpd-12-351-2012. Publisher: Copernicus GmbH. Accessed 2023-02-07

Kriegler E, Bauer N, Popp A, Humpenöder F, Leimbach M, Strefler J, Baumstark L, Bodirsky BL, Hilaire J, Klein D, Mouratiadou I, Weindl I, Bertram C, Dietrich J-P, Luderer G, Pehl M, Pietzcker R, Piontek F, Lotze-Campen H, Biewald A, Bonsch M, Giannousakis A, Kreidenweis U, Müller C, Rolinski S, Schultes A, Schwanitz J, Stevanovic M, Calvin K, Emmerling J, Fujimori S, Edenhofer O (2017) Fossil-fueled development (SSP5): an energy and resource intensive scenario for the 21st century. Global Environ Change 42:297–315. https://doi.org/10.1016/j.gloenvcha.2016.05.015. Accessed 2023-04-26

Lin Y, Wang Y, Hsieh J-S, Jiang JH, Su Q, Zhao L, Lavallee M, Zhang R (2023) Assessing the destructiveness of tropical cyclones induced by anthropogenic aerosols in an atmosphere-ocean coupled framework. Atmos Chem Phys 23(21):13835–13852. https://doi.org/10.5194/acp-23-13835-2023. Publisher: Copernicus GmbH. Accessed 2023-11-20

Liu X, Ma P-L, Wang H, Tilmes S, Singh B, Easter RC, Ghan SJ, Rasch PJ (2016) Description and evaluation of a new four-mode version of the Modal Aerosol Module (MAM4) within version 5.3 of the Community Atmosphere Model. Geosci Model Develop 9(2), 505–522. https://doi.org/10.5194/gmd-9-505-2016. Publisher: Copernicus GmbH. Accessed 2023-10-25

Liu M, Vecchi GA, Smith JA, Knutson TR (2019) Causes of large projected increases in hurricane precipitation rates with global warming. NPJ Climate Atmos Sci 2(1):1–5. https://doi.org/10.1038/s41612-019-0095-3. Number: 1 Publisher: Nature Publishing Group. Accessed 2022-09-16

Lonfat M, Marks FD, Chen SS (2004) Precipitation distribution in tropical cyclones using the tropical rainfall measuring mission (TRMM) microwave imager: a global perspective. Monthly Weather Rev 132(7):1645–1660. https://doi.org/10.1175/1520-0493(2004)132<1645:PDITCU>2.0.CO;2. Publisher: American Meteorological Society Section: Monthly Weather Review. Accessed 2023-08-16

Lund MT, Myhre G, Samset BH (2019) Anthropogenic aerosol forcing under the Shared Socioeconomic Pathways. Atmos Chem Phys 19(22):13827–13839. https://doi.org/10.5194/acp-19-13827-2019. Publisher: Copernicus GmbH. Accessed 2022-12-19

Mann ME, Emanuel KA (2006) Atlantic hurricane trends linked to climate change. Eos Trans Am Geophys Union 87(24):233–241. https://doi.org/10.1029/2006EO240001. _eprint: https://onlinelibrary.wiley.com/doi/pdf/10.1029/2006EO240001. Accessed 2024-03-08

Molinari J, Vollaro D (2013) What percentage of western north Pacific tropical cyclones form within the monsoon trough? Monthly Weather Rev 141(2):499–505. https://doi.org/10.1175/MWR-D-12-00165.1. Publisher: American Meteorological Society Section: Monthly Weather Review. Accessed 2024-03-08

Moon S, Ha K-J (2020) Future changes in monsoon duration and precipitation using CMIP6. NPJ Climate Atmos Sci 3(1):1–7. https://doi.org/10.1038/s41612-020-00151-w. Publisher: Nature Publishing Group. Accessed 2024-03-08

Moon Y, Kim D, Wing AA, Camargo SJ, Zhao M, Leung LR, Roberts MJ, Cha D-H, Moon J (2022a) An evaluation of tropical cyclone rainfall structures in the HighResMIP simulations against satellite observations. J Climate 35(22):7315–7338. https://doi.org/10.1175/JCLI-D-21-0564.1. Place: Boston MA, USA Publisher: American Meteorological Society

Moon Y, Kim D, Wing AA, Camargo SJ, Zhao M, Leung LR, Roberts MJ, Cha D-H, Moon J (2022b) An evaluation of tropical cyclone rainfall structures in the HighResMIP simulations against satellite observations. J Climate 35(22):7315–7338. https://doi.org/10.1175/JCLI-D-21-0564.1. Publisher: American Meteorological Society Section: Journal of Climate. Accessed 2024-02-19

Murakami H (2022a) Substantial global influence of anthropogenic aerosols on tropical cyclones over the past 40 years. Sci Adv 8(19):9493. https://doi.org/10.1126/sciadv.abn9493. Publisher: American Association for the Advancement of Science. Accessed 2022-07-07

Murakami H (2022b) Substantial global influence of anthropogenic aerosols on tropical cyclones over the past 40 years. Sci Adv 8(19):9493. https://doi.org/10.1126/sciadv.abn9493. Publisher: American Association for the Advancement of Science. Accessed 2022-07-19

Murakami H, Wang B (2022) Patterns and frequency of projected future tropical cyclone genesis are governed by dynamic effects. Commun Earth Environ 3(1):1–10. https://doi.org/10.1038/s43247-022-00410-z. Number: 1 Publisher: Nature Publishing Group. Accessed 2022-04-25

Murakami H, Delworth TL, Cooke WF, Zhao M, Xiang B, Hsu P-C (2020) Detected climatic change in global distribution of tropical cyclones. Proc Natl Acad Sci 117(20):10706–10714. https://doi.org/10.1073/pnas.1922500117. Publisher: National Academy of Sciences Section: Physical Sciences. Accessed 2021-09-03

Murphy LN, Bellomo K, Cane M, Clement A (2017) The role of historical forcings in simulating the observed Atlantic multidecadal oscillation. Geophys Res Lett 44(5):2472–2480. https://doi.org/10.1002/2016GL071337. _eprint: https://onlinelibrary.wiley.com/doi/pdf/10.1002/2016GL071337. Accessed 2024-05-14

Murphy LN, Klavans JM, Clement AC, Cane MA (2021) Investigating the roles of external forcing and ocean circulation on the Atlantic multidecadal SST variability in a large ensemble climate model hierarchy. J Clim 34(12):4835–4849. https://doi.org/10.1175/JCLI-D-20-0167.1

Nie J, Sobel AH (2016) Modeling the interaction between quasi-geostrophic vertical motion and convection in a single column. J Atmos Sci 73:1101–1117

Nie J, Sobel AH, Shaevitz DA, Wang S (2018) Dynamic amplification of extreme precipitation sensitivity. Proc Natl Acad Sci. https://doi.org/10.1073/pnas.1800357115

NOAA (2022) National centers for environmental information (NCEI) U.S. Billion-Dollar Weather and Climate Disasters. https://www.ncei.noaa.gov/access/billions/. https://doi.org/10.25921/stkw-7w73

Patricola CM, Wehner MF (2018) Anthropogenic influences on major tropical cyclone events. Nature 563(7731), 339–346. https://doi.org/10.1038/s41586-018-0673-2. Bandiera_abtest: a Cg_type: Nature Research Journals Number: 7731 Primary_atype: Research Publisher: Nature Publishing Group Subject_term: Attribution; Climate and Earth system modelling; Projection and prediction Subject_term_id: attribution;climate-and-earth-system-modelling;projection-and-prediction. Accessed 2021-07-23

Prabhat RO, Byna S, Wu K, Li F, Wehner M, Bethel W (2012) TECA: a parallel toolkit for extreme climate analysis. Proc Comput Sci 9:866–876. https://doi.org/10.1016/j.procs.2012.04.093

Prat OP, Nelson BR (2013) Precipitation contribution of tropical cyclones in the southeastern United States from 1998 to 2009 using TRMM satellite data. J Climate 26(3):1047–1062. https://doi.org/10.1175/JCLI-D-11-00736.1. Publisher: American Meteorological Society Section: Journal of Climate. Accessed 2023-06-12

Qian Y, Guo Z, Larson VE, Leung LR, Lin W, Ma P-L, Wan H, Wang H, Xiao H, Xie S, Yang B, Zhang K, Zhang S, Zhang Y (2023) Region and cloud regime dependence of parametric sensitivity in E3SM atmosphere model. Climate Dyn. https://doi.org/10.1007/s00382-023-06977-3. Accessed 2023-11-28

Rappaport EN (2014) Fatalities in the United States from Atlantic tropical cyclones: new data and interpretation. Bull Am Meteorol Soc 95(3):341–346. https://doi.org/10.1175/BAMS-D-12-00074.1. Publisher: American Meteorological Society Section: Bulletin of the American Meteorological Society. Accessed 2023-01-19

Rao S, Klimont Z, Smith SJ, Van Dingenen R, Dentener F, Bouwman L, Riahi K, Amann M, Bodirsky BL, Vuuren DP, Aleluia Reis L, Calvin K, Drouet L, Fricko O, Fujimori S, Gernaat D, Havlik P, Harmsen M, Hasegawa T, Heyes C, Hilaire J, Luderer G, Masui T, Stehfest E, Strefler J, Sluis S, Tavoni M (2017) Future air pollution in the shared socio-economic pathways. Global Environ Change 42:346–358. https://doi.org/10.1016/j.gloenvcha.2016.05.012. Accessed 2024-01-18

Rayner NA, Parker DE, Horton EB, Folland CK, Alexander LV, Rowell DP, Kent EC, Kaplan A (2003) Global analyses of sea surface temperature, sea ice, and night marine air temperature since the late nineteenth century. J Geophys Res Atmos 108(D14). https://doi.org/10.1029/2002JD002670. _eprint: https://onlinelibrary.wiley.com/doi/pdf/10.1029/2002JD002670. Accessed 2022-03-01

Riahi K, Vuuren DP, Kriegler E, Edmonds J, O'Neill BC, Fujimori S, Bauer N, Calvin K, Dellink R, Fricko O, Lutz W, Popp A, Cuaresma JC, Kc S, Leimbach M, Jiang L, Kram T, Rao S, Emmerling J, Ebi K, Hasegawa T, Havlik P, Humpenöder F, Da Silva LA, Smith S, Stehfest E, Bosetti V, Eom J, Gernaat D, Masui T, Rogelj J, Strefler J, Drouet L, Krey V, Luderer G, Harmsen M, Takahashi K, Baumstark L, Doelman JC, Kainuma M, Klimont Z, Marangoni G, Lotze-Campen H, Obersteiner M, Tabeau A, Tavoni M (2017) The Shared Socioeconomic Pathways and their energy, land use, and greenhouse gas emissions implications: an overview. Global Environ Change 42:153–168. https://doi.org/10.1016/j.gloenvcha.2016.05.009. Accessed 2024-01-18

Roberts MJ, Camp J, Seddon J, Vidale PL, Hodges K, Vannière B, Mecking J, Haarsma R, Bellucci A, Scoccimarro E, Caron L-P, Chauvin F, Terray L, Valcke S, Moine M-P, Putrasahan D, Roberts CD, Senan R, Zarzycki C, Ullrich P, Yamada Y, Mizuta R, Kodama C, Fu D, Zhang Q, Danabasoglu G, Rosenbloom N, Wang H, Wu L (2020) Projected future changes in tropical cyclones using the CMIP6 HighResMIP multimodel ensemble. Geophys Res Lett 47(14):2020–088662. https://doi.org/10.1029/2020GL088662. _eprint: https://onlinelibrary.wiley.com/doi/pdf/10.1029/2020GL088662. Accessed 2022-08-23

Rosenfeld D, Woodley WL, Khain A, Cotton WR, Carrió G, Ginis I, Golden JH (2012) Aerosol effects on microstructure and intensity of tropical cyclones. Bull Am Meteorol Soc 93(7):987–1001. https://doi.org/10.1175/BAMS-D-11-00147.1. Publisher: American Meteorological Society Section: Bulletin of the American Meteorological Society. Accessed 2022-11-10

Rousseau-Rizzi R, Emanuel K (2022) Natural and anthropogenic contributions to the hurricane drought of the 1970s–1980s. Nat Commun 13(1):5074. https://doi.org/10.1038/s41467-022-32779-y. Number: 1 Publisher: Nature Publishing Group. Accessed 2022-09-03

Russotto RD, Strong JDO, Camargo SJ, Sobel A, Elsaesser GS, Kelley M, Del Genio A, Moon Y, Kim D (2022) Evolution of tropical cyclone properties across the development cycle of the GISS-E3 global climate model. J Adv Model Earth Syst 14(1):2021–002601. https://doi.org/10.1029/2021MS002601. _eprint: https://onlinelibrary.wiley.com/doi/pdf/10.1029/2021MS002601. Accessed 2024-03-11

Saha A, Ghosh S (2019) Can the weakening of Indian Monsoon be attributed to anthropogenic aerosols? Environ Res Commun 1(6):061006. https://doi.org/10.1088/2515-7620/ab2c65. Publisher: IOP Publishing. Accessed 2022-09-01

Schade LR, Emanuel KA (1999) The ocean's effect on the intensity of tropical cyclones: results from a simple coupled atmosphere-ocean model. J Atmos Sci 56(4):642–651. https://doi.org/10.1175/1520-0469(1999)056<0642:TOSEOT>2.0.CO;2. Publisher: American Meteorological Society Section: Journal of the Atmospheric Sciences. Accessed 2022-06-14

Scoccimarro E, Gualdi S, Villarini G, Vecchi GA, Zhao M, Walsh K, Navarra A (2014) Intense precipitation events associated with landfalling tropical cyclones in response to a warmer climate and increased CO_2. J Climate 27(12):4642–4654. https://doi.org/10.1175/JCLI-D-14-00065.1. Publisher: American Meteorological Society Section: Journal of Climate. Accessed 2023-03-20

Sena ACT, Patricola CM, Loring B (2022) Future changes in active and inactive Atlantic hurricane seasons in the energy Exascale earth system model. Geophys Res Lett 49(21):2022–100267. https://doi.org/10.1029/2022GL100267. _eprint: https://onlinelibrary.wiley.com/doi/pdf/10.1029/2022GL100267. Accessed 2022-11-10

Sharmila S, Walsh KJE (2018) Recent poleward shift of tropical cyclone formation linked to Hadley cell expansion. Nat Clim Change 8(8):730–736. https://doi.org/10.1038/s41558-018-0227-5. Number: 8 Publisher: Nature Publishing Group. Accessed 2022-11-14

Shearer EJ, Afzali Gorooh V, Nguyen P, Hsu K-L, Sorooshian S (2022) Unveiling four decades of intensifying precipitation from tropical cyclones using satellite measurements. Sci Rep 12(1):13569. https://doi.org/10.1038/s41598-022-17640-y. Number: 1 Publisher: Nature Publishing Group. Accessed 2023-02-01

Shekhar M, Sharma A, Pandey P, Sharma A, Dimri AP (2024) Assessing the past and future dynamics of the Asian summer monsoon: Insights from palaeomonsoon synthesis and CMIP6 data. Global Environ Change Adv 2:100004. https://doi.org/10.1016/j.gecadv.2023.100004. Accessed 2024-03-11

Singh VK, Roxy MK (2022) A review of ocean-atmosphere interactions during tropical cyclones in the north Indian Ocean. Earth Sci Rev 226:103967. https://doi.org/10.1016/j.earscirev.2022.103967. Accessed 2022-04-26

Sobel AH, Camargo SJ, Hall TM, Lee C-Y, Tippett MK, Wing AA (2016) Human influence on tropical cyclone intensity. Science 353(6296):242–246. https://doi.org/10.1126/science.aaf6574. Publisher: American Association for the Advancement of Science Section: Review. Accessed 2021-07-27

Sobel AH, Camargo SJ, Previdi M (2019) Aerosol versus greenhouse gas effects on tropical cyclone potential intensity and the hydrologic cycle. J Climate 32(17):5511–5527. https://doi.org/10.1175/JCLI-D-18-0357.1. Accessed 2021-07-26

Sobel AH, Wing AA, Camargo SJ, Patricola CM, Vecchi GA, Lee C-Y, Tippett MK (2021) Tropical cyclone frequency. Earth's Future 9(12):2021–002275. https://doi.org/10.1029/2021EF002275. Accessed 2022-02-01

Sobel AH, Lee C-Y, Bowen SG, Camargo SJ, Cane MA, Clement A, Fosu B, Hart M, Reed KA, Seager R, Tippett MK (2023) Near-term tropical cyclone risk and coupled Earth system model biases. Proc Natl Acad Sci 120(33):2209631120. https://doi.org/10.1073/pnas.2209631120. Publisher: Proceedings of the National Academy of Sciences. Accessed 2024-03-15

Stansfield AM, Reed KA (2021) Tropical cyclone precipitation response to surface warming in Aquaplanet simulations with uniform thermal forcing. J Geophys Res Atmos 126(24):2021–035197. https://doi.org/10.1029/2021JD035197. _eprint: https://onlinelibrary.wiley.com/doi/pdf/10.1029/2021JD035197. Accessed 2023-01-17

Studholme J, Fedorov AV, Gulev SK, Emanuel K, Hodges K (2022) Poleward expansion of tropical cyclone latitudes in warming climates. Nat Geosci 15(1):14–28. https://doi.org/10.1038/s41561-021-00859-1. Number: 1 Publisher: Nature Publishing Group. Accessed 2022-07-05

Szopa S, Naik V, Adhikary B, Artaxo P, Berntsen T, Collins WD, Fuzzi S, Gallardo L, Kiendler-Scharr A, Klimont Z, Liao H, Unger N, Zanis P (2021) Short-lived climate forcers. In: Masson-Delmotte V, Zhai P, Pirani A, Connors SL, Péan C, Berger S, Caud N, Chen Y, Goldfarb L, Gomis MI, Huang M, Leitzell K, Lonnoy E, Matthews JBR, Maycock TK, Waterfield T, Yelekçi O, Yu R, Zhou B (eds) Climate change 2021: the physical science basis. Contribution of working group I to the sixth assessment report of the intergovernmental panel on climate change, pp 817–922. Cambridge University Press, Cambridge, United Kingdom and New York, NY, USA. https://doi.org/10.1017/9781009157896.008. Type: Book Section

Takahashi C, Watanabe M, Mori M (2017) Significant aerosol influence on the recent decadal decrease in tropical cyclone activity over the western North Pacific. Geophys Res Lett 44(18):9496–9504. https://doi.org/10.1002/2017GL075369. _eprint: https://onlinelibrary.wiley.com/doi/pdf/10.1002/2017GL075369. Accessed 2023-01-24

Taylor KE, Stouffer RJ, Meehl GA (2012) An overview of CMIP5 and the experiment design. Bull Am Meteorol Soc 93(4):485–498. https://doi.org/10.1175/BAMS-D-11-00094.1. Publisher: American Meteorological Society Section: Bulletin of the American Meteorological Society. Accessed 2024-01-18

Thornhill GD, Collins WJ, Kramer RJ, Olivié D, Skeie RB, O'Connor FM, Abraham NL, Checa-Garcia R, Bauer SE, Deushi M, Emmons LK, Forster PM, Horowitz LW, Johnson B, Keeble J, Lamarque J-F, Michou M, Mills MJ, Mulcahy JP, Myhre G, Nabat P, Naik V, Oshima N, Schulz M, Smith CJ, Takemura T, Tilmes S, Wu T, Zeng G, Zhang J (2021) Effective radiative forcing from emissions of reactive gases and aerosols—a multi-model comparison. Atmos Chem Phys 21(2):853–874. https://doi.org/10.5194/acp-21-853-2021. Publisher: Copernicus GmbH. Accessed 2024-03-11

Ting M, Camargo SJ, Li C, Kushnir Y (2015) Natural and forced north atlantic hurricane potential intensity change in CMIP5 models. J Climate 28(10):3926–3942. https://doi.org/10.1175/JCLI-D-14-00520.1. Publisher: American Meteorological Society Section: Journal of Climate. Accessed 2024-01-18

Traxl D, Boers N, Rheinwalt A, Bookhagen B (2021) The role of cyclonic activity in tropical temperature-rainfall scaling. Nat Commun 12(1):6732. https://doi.org/10.1038/s41467-021-27111-z. Number: 1 Publisher: Nature Publishing Group. Accessed 2023-01-17

Tu S, Xu J, Chan JCL, Huang K, Xu F, Chiu LS (2021) Recent global decrease in the inner-core rain rate of tropical cyclones. Nat Commun 12(1):1948. https://doi.org/10.1038/s41467-021-22304-y. Number: 1 Publisher: Nature Publishing Group. Accessed 2023-02-01

Vecchi GA, Delworth TL, Murakami H, Underwood SD, Wittenberg AT, Zeng F, Zhang W, Baldwin JW, Bhatia KT, Cooke W, He J, Kapnick SB, Knutson TR, Villarini G, Wiel K, Anderson W, Balaji V, Chen J, Dixon KW, Gudgel R, Harris LM, Jia L, Johnson NC, Lin S-J, Liu M, Ng CHJ, Rosati A, Smith JA, Yang X (2019) Tropical cyclone sensitivities to CO_2 doubling: roles of atmospheric resolution, synoptic variability and background climate changes. Climate Dyn 53(9):5999–6033. https://doi.org/10.1007/s00382-019-04913-y. Accessed 2022-08-22

Villafuerte MQ, Lambrento JCR, Hodges KI, Cruz FT, Cinco TA, Narisma GT (2021) Sensitivity of tropical cyclones to convective parameterization schemes in RegCM4. Clim Dyn 56(5):1625–1642. https://doi.org/10.1007/s00382-020-05553-3. Accessed 2023-11-20

Villarini G, Lavers DA, Scoccimarro E, Zhao M, Wehner MF, Vecchi GA, Knutson TR, Reed KA (2014) Sensitivity of tropical cyclone rainfall to idealized global-scale forcings. J Clim 27(12):4622–4641. https://doi.org/10.1175/JCLI-D-13-00780.1. Publisher: American Meteorological Society Section: Journal of Climate. Accessed 2023-01-19

Vitart F, Stockdale TN (2001) Seasonal forecasting of tropical storms using coupled GCM integrations. Monthly Weather Rev 129(10):2521–2537. https://doi.org/10.1175/1520-0493(2001)129<2521:SFOTSUspsdoigtsps2.0.CO;2. Publisher: American Meteorological Society Section: Monthly Weather Review. Accessed 2022-04-04

Vuuren DP, Stehfest E, Gernaat DEHJ, Doelman JC, Berg M, Harmsen M, Boer HS, Bouwman LF, Daioglou V, Edelenbosch OY, Girod B, Kram T, Lassaletta L, Lucas PL, Meijl H, Müller C, Ruijven BJ, Sluis S, Tabeau A (2017) Energy, land-use and greenhouse gas emissions trajectories under a green growth paradigm. Global Environ Change 42:237–250. https://doi.org/10.1016/j.gloenvcha.2016.05.008. Accessed 2024-01-18

Walsh KJE, McBride JL, Klotzbach PJ, Balachandran S, Camargo SJ, Holland G, Knutson TR, Kossin JP, Lee T-C, Sobel A, Sugi M (2016) Tropical cyclones and climate change. WIREs Clim Change 7(1):65–89. https://doi.org/10.1002/wcc.371. Accessed 2021-07-23

Wang Y, Lee K-H, Lin Y, Levy M, Zhang R (2014) Distinct effects of anthropogenic aerosols on tropical cyclones. Nat Clim Change 4(5):368–373. https://doi.org/10.1038/nclimate2144. Number: 5 Publisher: Nature Publishing Group. Accessed 2022-10-07

Wang C, Soden BJ, Yang W, Vecchi GA (2021) Compensation between cloud feedback and aerosol-cloud interaction in CMIP6 models. Geophys Res Lett 48(4):2020–091024. https://doi.org/10.1029/2020GL091024. _eprint: https://onlinelibrary.wiley.com/doi/pdf/10.1029/2020GL091024. Accessed 2023-11-29

Weng J, Wang L, Luo J, Chen B, Peng X, Gan Q (2022) A contrast of the monsoon-tropical cyclone relationship between the Western and Eastern North Pacific. Atmosphere 13(9):1465. https://doi.org/10.3390/atmos13091465. Number: 9 Publisher: Multidisciplinary Digital Publishing Institute. Accessed 2024-03-08

Westervelt DM, Horowitz LW, Naik V, Golaz J-C, Mauzerall DL (2015) Radiative forcing and climate response to projected 21st century aerosol decreases. Atmos Chem Phys 15(22):12681–12703. https://doi.org/10.5194/acp-15-12681-2015. Publisher: Copernicus GmbH. Accessed 2023-11-29

Xie S, Wang Y-C, Lin W, Ma H-Y, Tang Q, Tang S, Zheng X, Golaz J-C, Zhang GJ, Zhang M (2019) Improved diurnal cycle of precipitation in E3SM with a revised convective triggering function. J Adv Model Earth Syst 11(7):2290–2310. https://doi.org/10.1029/2019MS001702. _eprint: https://onlinelibrary.wiley.com/doi/pdf/10.1029/2019MS001702. Accessed 2023-10-12

Xu Y, Lamarque J-F, Sanderson BM (2018) The importance of aerosol scenarios in projections of future heat extremes. Clim Change 146(3):393–406. https://doi.org/10.1007/s10584-015-1565-1. Accessed 2023-11-29

Yan X, Zhang R, Knutson TR (2017) The role of Atlantic overturning circulation in the recent decline of Atlantic major hurricane frequency. Nat Commun 8(1):1695. https://doi.org/10.1038/s41467-017-01377-8. Publisher: Nature Publishing Group. Accessed 2024-05-14

Yoshimura J, Sugi M (2005) Tropical cyclone climatology in a high-resolution AGCM—impacts of SST warming and CO<SUBspsdoigtsps2</SUBspsdoigtsps Increase–. Sola 1:133–136. https://doi.org/10.2151/sola.2005-035

Zhang GJ, McFarlane NA (1995) Sensitivity of climate simulations to the parameterization of cumulus convection in the Canadian climate centre general circulation model. Atmos Ocean 33(3):407–446. https://doi.org/10.1080/07055900.1995.9649539. Publisher: Taylor & Francis. Accessed 2023-10-12

Zhang C, Wang Y (2018) Why is the simulated climatology of tropical cyclones so sensitive to the choice of cumulus parameterization scheme in the WRF model? Clim Dyn 51(9):3613–3633. https://doi.org/10.1007/s00382-018-4099-1. Accessed 2023-11-20

Zhang R, Delworth TL, Sutton R, Hodson DLR, Dixon KW, Held IM, Kushnir Y, Marshall J, Ming Y, Msadek R, Robson J, Rosati AJ, Ting M, Vecchi GA (2013) Have aerosols caused the observed Atlantic multidecadal variability? J Atmos Sci 70(4):1135–1144. https://doi.org/10.1175/JAS-D-12-0331.1. Publisher: American Meteorological Society Section: Journal of the Atmospheric Sciences. Accessed 2024-05-14

Zhang H, He H, Zhang W-Z, Tian D (2021) Upper ocean response to tropical cyclones: a review. Geosci Lett 8(1):1. https://doi.org/10.1186/s40562-020-00170-8. Accessed 2024-05-14

Zhao M, Held IM, Lin S-J (2012) Some counterintuitive dependencies of tropical cyclone frequency on parameters in a GCM. J Atmos Sci 69(7):2272–2283. https://doi.org/10.1175/JAS-D-11-0238.1. Publisher: American Meteorological Society Section: Journal of the Atmospheric Sciences. Accessed 2023-11-20

Zhao C, Lin Y, Wu F, Wang Y, Li Z, Rosenfeld D, Wang Y (2018) Enlarging rainfall area of tropical cyclones by atmospheric aerosols. Geophys Res Lett 45(16):8604–8611. https://doi.org/10.1029/2018GL079427. _eprint: https://onlinelibrary.wiley.com/doi/pdf/10.1029/2018GL079427. Accessed 2022-09-16

Zhou C, Lu J, Hu Y, Zelinka MD (2020) Responses of the Hadley circulation to regional sea surface temperature changes. J Climate 33(2):429–441. https://doi.org/10.1175/JCLI-D-19-0315.1. Publisher: American Meteorological Society Section: Journal of Climate. Accessed 2024-03-18